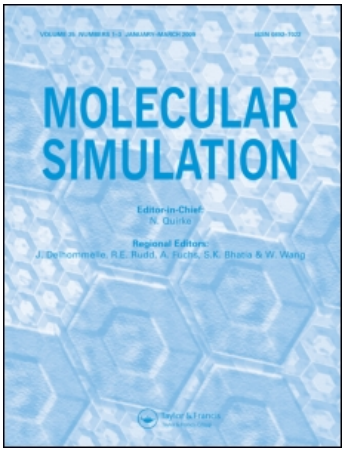

Molecular Simulation
Publication details, including instructions for authors and subscription information:
http://www.informaworld.com/smpp/title~content=t713644482

Molecular Dynamics Simulations of Adsorbed Alkanes in Silica Micropores at Low-to-Moderate Loadings

Karthik Raghavan[a]; J. M. D. Macelroy[b]
[a] School of Chemical Engineering, Purdue University, W. Lafayette, IN, USA [b] Department of Chemical Engineering, University College Dublin, Dublin 4, Ireland

To cite this Article Raghavan, Karthik and Macelroy, J. M. D.(1995) 'Molecular Dynamics Simulations of Adsorbed Alkanes in Silica Micropores at Low-to-Moderate Loadings', Molecular Simulation, 15: 1, 1 — 33
To link to this Article: DOI: 10.1080/08927029508022326
URL: http://dx.doi.org/10.1080/08927029508022326

Molecular Simulation, 1995, Vol. 15, pp. 1–33
Reprints available directly from the publisher
Photocopying permitted by license only

MOLECULAR DYNAMICS SIMULATIONS OF ADSORBED ALKANES IN SILICA MICROPORES AT LOW-TO-MODERATE LOADINGS

KARTHIK RAGHAVAN

School of Chemical Engineering, Purdue University, W. Lafayette, IN 47907, USA

J. M. D. MACELROY

Department of Chemical Engineering, University College Dublin, Belfield, Dublin 4, Ireland

(Received August 1994, accepted November 1994)

The configurational and dynamical properties of rigid and flexible alkanes adsorbed on microporous silica are investigated using molecular simulation techniques. Two isomeric alkanes, neopentane and n-pentane, are examined in detail over a range of surface coverages and temperatures using the RATTLE simulation algorithm in which the tetrahedrally rigid neopentane and linearly flexible n-pentane molecules are considered to be composed of C (neopentane), CH_2, and CH_3 Lennard-Jones sites. The solid adsorbent is atomistically modelled as a rigid medium using a technique which was shown in earlier work to provide a quantitatively realistic representation of microporous silica. The simulation results reveal the significant influence of intramolecular structure and dynamics on the properties of the adsorbed molecules. In particular, one of the features observed in the n-pentane simulations, which may have a direct bearing on the catalytic activity of silica, is a substantial broadening in the bond angle and dihedral angle distributions during adsorption onto the heterogeneous silica surface.

KEY WORDS: Adsorption, diffusion, alkanes, microporous silica

1 INTRODUCTION

In the past decade molecular dynamics computer simulation techniques have been widely used to investigate the behaviour of fluids confined within very fine pores. In much of the work reported to date the systems most frequently addressed have involved simple inhomogeneous fluids composed of structureless particles [1–11]. The intramolecular shape or structure of the micropore fluid has been taken into consideration in a number of cases [12–17], however the molecular models employed have, with exception of this work reported in [13, 16, 17], usually neglected intramolecular rotations and vibrations.

In this paper results obtained from a molecular dynamics simulation study of alkane vapors adsorbed on microporous silica are reported. The alkane/silica system was chosen for its comparative simplicity (intermolecular interactions within the fluid/solid system are adequately described by short-ranged London-van der Waals forces [10, 18, 19]) and in view of the availability of reliable intramolecular potential energy functions

for alkane systems [20–23]. With regard to the latter, simulation of alkanes permits an examination of the role of intramolecular bending and torsion in the transport mechanism and provides a convenient basis for investigating the influence of solid surfaces on the intramolecular conformations of flexible chain molecules.

The computational technique employed in this work is based on the RATTLE modification of the SHAKE algorithm [24] which has been successfully used in a wide variety of molecular simulation studies ranging from low molecular weight alkanes [20–23] to proteins and biopolymers [25–34]. This algorithm is readily applied to both rigid and flexible molecules, and is used here to investigate the influence of molecular shape and internal rotation on the dynamical properties of two confined isomeric alkanes, neopentane and n-pentane. The contrast between the spherically symmetric neopentane molecule and the linear n-pentane not only enables a quantitative analysis of the effects of intramolecular motion on transport in microporous media, but also permits a comparison with earlier studies reported for a structureless Lennard-Jones fluid [11] and a rigid needle fluid [14] in micropores.

The theoretical background and the molecular models employed here are briefly described in section 2. The simulation procedures and methods of analysis are also outlined in this section with particular attention given to the techniques used to characterize the intramolecular motion of the adsorbed alkanes. In section 3 the results obtained are discussed and, finally, in section 4 we provide a summary of our findings.

2 BACKGROUND THEORY AND SIMULATION TECHNIQUE

2.1 *Background Theory*

As in earlier work [11] we are primarily interested in elucidating the underlying mechanism governing translational diffusion of adsorbing vapors in microporous media. For the single component alkane systems under consideration in this paper, the tracer diffusion flux in the isotropic microporous silica medium is given by

$$\vec{J}_{1^*} = -\frac{n_{1^*}}{kT}\left[\frac{N}{N-1}(\Omega_{1^*1^*} - \Omega_{00})\right]\nabla_T \mu_{1^*} \tag{1}$$

where N is the total number of fluid particles in a macroscopically small though microscopically large element of the system (i.e. in volume V), μ_{1^*} is the tracer chemical potential, and n_{1^*} is its number density. The coefficients $\Omega_{1^*1^*}$ and Ω_{00} in Equation (1) are given by

$$\Omega_{1^*1^*} = \frac{1}{3N}\sum_{j=1}^{N}\int_0^\infty \langle \boldsymbol{v}_j(0)\cdot\boldsymbol{v}_j(t)\rangle dt \tag{2}$$

and

$$\Omega_{00} = \frac{1}{3N}\int_0^\infty \langle \boldsymbol{u}_0(0)\cdot\boldsymbol{u}_0(t)\rangle dt \tag{3}$$

where $\boldsymbol{v}_j(t)$ is the center of mass velocity of particle j and $\boldsymbol{u}_0(t)$ is the instantaneous center of mass velocity of the N-particle fluid as a whole at time t.

In addition to the tracer flux, we also consider the diffusion flux of the local micropore fluid which is given by

$$\vec{J}_A = \frac{n_A}{kT}[N\Omega_{oo}]\nabla_T \mu_A \tag{4}$$

where n_A and μ_A are the number density and chemical potential of the micropore fluid locally within the volume V. The combined term $N\Omega_{00}$ in Eqution (4) is the diffusion coefficient usually measured in permeation or gravimetric sorption experiments. In contrast, the quantity inside the square brackets of Equation (1) is most frequently referred to as the tracer diffusion coefficient which is measured using radioactive tracers or NMR spectroscopy. For notational purposes we will employ the following definitions

$$D_{AA} = N\Omega_{oo} \tag{5a}$$

and

$$D_{1^*1^*} = \frac{N}{N-1}(\Omega_{1^*1^*} - \Omega_{00}) \tag{5b}$$

For absorbing vapors composed of molecules with a well defined internal structure, a variety of additional properties may be investigated to ascertain the role of the internal degrees of freedom in the diffusion process and to determine the influence of the solid surface on the configurational and dynamical states of the particles. Of particular interest are the time-correlation functions

$$P_1 = \langle \boldsymbol{u}(0)\cdot\boldsymbol{u}(t)\rangle \tag{6a}$$

and

$$P_2 = \left\langle \frac{3}{2}(\boldsymbol{u}(0)\cdot\boldsymbol{u}(t))^2 - \frac{1}{2} \right\rangle \tag{6b}$$

where $\boldsymbol{u}$ is a unit vector along a given axis within a molecule. The terms within the angular brackets are Legendre polynomials of the first and second kinds, respectively. Gordon [35, 36] has shown that P_1 and P_2 may be determined from spectroscopic data. The correlation function P_1 is obtained directly from the inverse Fourier transform of the infrared spectrum of the molecules, and P_2 is determined in a similar manner from the depolarized part of the Raman spectrum. NMR spectroscopy may also be used to obtain a limited amount of information on the behavior of the correlation function P_2 [36].

Other dynamical properties of interest include the angular momentum autocorrelation function and its integral as defined by

$$\boldsymbol{D}_J = \frac{1}{3N}\sum_{i=1}^{N}\int_0^{\infty}\langle \boldsymbol{J}_i(0)\cdot\boldsymbol{J}_i(t)\rangle dt \tag{7}$$

wher $\boldsymbol{J}_i(t)$ is the angular momentum vector given by

$$\boldsymbol{J}_i = \sum_{k=1}^{N_{si}} m_k(\boldsymbol{r}_{ki}-\boldsymbol{r}_i)\times(\boldsymbol{v}_{ki}-\boldsymbol{v}_i) \tag{8}$$

N_{Si}, m_k, $\boldsymbol{r}_{ki}$ and $\boldsymbol{v}_{ki}$ in Equation (8) are respectively, the number of atoms or sites in the molecule i, the mass of site k, and the position and velocity vectors of site k. The center of mass position vector of molecule i as a whole is $\boldsymbol{r}_i$.

For rigid molecules Equation (7) may be used to determine the rotational diffusion coefficient, $\boldsymbol{D}_r$ [38] which, in turn, is directly related to the orientational correlation functions P_1 and P_2. For flexible particles it is still possible to use the definition of $\boldsymbol{D}_J$ given in Equation (7); however, since the moments of inertia are not easily determined in this case, the evaluation of a rotational diffusion coefficient is not a straightforward task. In the computations to be discussed below, we have determined $\boldsymbol{D}_J$ for each of the adsorbing vapors considered here. The correlation functions P_1 and P_2 have also been calculated for selected site-site bonds within the rigid neopentane molecule and the flexible n-pentane particle, the molecular models of which will be considered in greater detail in section 2.2.

For the flexible n-pentane system a number of additional properties exist which are examined in this work. These include the time-correlation functions defined by

$$\rho(\cos\phi) = \frac{\langle\cos\phi(0)\cdot\cos\phi(t)\rangle - \langle\cos\phi(0)\rangle^2}{\langle\cos^2\phi(0)\rangle - \langle\cos\phi(0)\rangle^2} \tag{9}$$

$$\rho_1 = \frac{\langle r^2(0)\,r^2(t)\rangle - \langle r^2(0)\rangle^2}{\langle r^4(0)\rangle - \langle r^2(0)\rangle^2} \tag{10}$$

and

$$\rho_2 = \frac{\langle s^2(0)\,s^2(t)\rangle - \langle s^2(0)\rangle^2}{\langle s^4(0)\rangle - \langle s^2(0)\rangle^2} \tag{11}$$

where r is the dihedral angle generated by three adjacent bonds within a given n-pentane particle, and r^2 and s^2 are the squares of the end-to-end distance and radius of gyration of the particle respectively with s given by

$$\left\|\mathbf{s}_j = \frac{1}{\boldsymbol{M}_j}\sum_{i=1}^{N_{sj}}(\mathbf{r}_{ij}-\mathbf{r}_j)\right\| \tag{12}$$

The functions defined in Equations (9)–(11) are sensitive indicators of the influence of the immediate environment on the intramolecular conformational transitions which determine the average shape of the n-pentane particles and the manner in which this component diffuses through the microporous medium.

In addition to dynamical quantities described above, a further source of information is provided by the configurational properties of the micropore fluid. For example, the fluid/solid density profiles and/or radial distribution functions are evaluated here to assist in determining the most probable locations of the fluid particles. Furthermore, the average orientation of the alkane molecules near the solid surface can be characterized by considering bond vector projections. For the rigid tetrahedrally structured neopentane we use

$$\cos \Psi_i = \boldsymbol{e}_{ic} \cdot \boldsymbol{e}_{if} \tag{13a}$$

$$\cos \chi_i = \boldsymbol{e}_{ic} \cdot \boldsymbol{e}_{in} \tag{13b}$$

where $\boldsymbol{e}_{ic}$ is the unit vector from the center of mass of the ith molecule normal to the solid surface, and $\boldsymbol{e}_{if}$ and $\boldsymbol{e}_{in}$ are, respectively, the unit vectors from the center of mass of the molecule to the carbon atom farthest from, and nearest to the solid surface. The configurational state of the n-pentane particles is also investigated using

$$\cos \zeta_i = \boldsymbol{e}_{ic} \cdot \boldsymbol{e}_n \tag{14}$$

where $\boldsymbol{e}_n$ is the unit vector along the line joining the midpoints of the first and last bonds in a given molecule. For the moderately short n-pentane chain under consideration here the angle ζ is useful in determining its average orientation near the solid surface.

The equilibrium conformational states of n-pentane as depicted by the time-averaged bending and torsion angle distributions are also of interest since the solid adsorbent is expected to have a significant effect due to the size of the smallest pore openings (~ 4 Å–5 Å) and the adsorptive potential field of the heterogeneous porous medium involved in these studies. For similar reasons, the averaged end-to-end distance r, and the radius of gyration s of the molecules in the adsorbed state were also determined for comparison with the bulk ideal vapor phase.

2.2 *Molecular Models and Simulation Technique*

The model of the microporous silica medium employed here has been described in detail in earlier work [11]. Briefly, the micropore structure is generated by randomly distributed, nonoverlapping, interconnected microspheres of vitreous SiO_2. The average microsphere radius is 13.8 Å, which is considered to typify the size of the silica particles which make up the solid backbone of microporous silica [10, 11]. The average number of silicon atoms and oxygen atoms in each sphere is 235.3 and 539.3, respectively. The excess oxygen content is associated with the singly bonded surface oxygen atoms which we here consider to represent the surface hydroxyl groups normally present in virgin silica gel. In the simulations conducted in this work we have employed the same periodically-imaged fundamental cell of silica microspheres as used

in Ref. [11]. This cell contains eight silica spheres [11] which is believed to be large enough to be statistically representative sample of a macroscopic silica medium while it is small enough to accommodate a manageable number of alkane molecules adsorbed at low to moderate loadings.

The alkane particles themselves are modeled as beaded structures composed of spherically symmetric Lennard-Jones sites, five sites in the case of neopentane (the central carbon and four tetrahedrally located methyl groups) and five sites for the linear n-pentane (3 methylene groups and 2 methyl end groups). Previous studies [39, 40] of alkanes indicate that the assumption of structureless methylene and methyl groups is not unreasonable although care must be exercised with regard to the manner in which these groups interact intramolecularly. In this work we assume the neopentane particles are rigid (fixed bond lengths and fixed bond angles). In the case of the n-pentane particle, however, only the bond lengths are constrained with the bending modes described by the harmonic potential [40]

$$\Phi_\theta = k_\theta(\cos\theta - \cos\theta_0)^2 \tag{15}$$

and the torsional motion is governed by the potential [23]

$$\Phi_\phi = \sum_{i=0}^{5} C_i \cos^i \phi \tag{16}$$

The constant k_θ in Equation (15) and the constants $C_i (i = 1..5)$ in Equation (16) were taken as $k_\theta = 130\,\text{kJ/mol}$, $C_0 = 1116.0$, $C_1 = 1462.0$, $C_2 = -1578.0$, $C_3 = -368.0$, $C_4 = 3156.0$ and $C_5 = -3788.0$. The value for k_θ is based on a result from Consistent Force Field theory [41] while the parameters for the dihedral potential function in Equation (16) are those reported by Ryckaert and Bellemans [21]. The average bond angle θ_0 in the bending potential was taken as 109° 28′.

The structureless Lennard-Jones (12-6) methyl and methylene sites are only distinguished by their masses ($m_{CH_3} = 15.035$ a.m.u. and $m_{CH_2} = 14.027$ a.m.u.) while their LJ potential parameters are assumed to be the same, $\sigma_{MeMe} = 3.923\,\text{Å}$ and $\varepsilon_{MeMe}/k = 72\,\text{K}$ [39]. In the case of neopentane the tertiary carbon (C) has a smaller LJ diameter of 3.207 Å [42] and ε_{CC}/k is estimated from the Kirkwood-Müller formula

$$A_{ij} = \frac{3}{2} e^2 a_0^{1/2} \frac{\alpha_i \alpha_j}{\sqrt{\frac{\alpha_i}{n_i}} + \sqrt{\frac{\alpha_j}{n_j}}} \tag{17}$$

where A_{ij} is related to the well depth ε_{ij} appearing in the LJ (12-6) potential

$$\Phi_{ij}^{LJ} = 4\varepsilon_{ij}\left[\left(\frac{\sigma_{ij}}{r_{ij}}\right)^{12} - \left(\frac{\sigma_{ij}}{r_{ij}}\right)^{6}\right] \tag{18}$$

via the expression

$$A_{ij} = 4\varepsilon_{ij}\sigma_{ij}^6 \tag{19}$$

The quantities e, a_0, α_i and n_i are respectively, the charge on the electron, the Bohr radius, the polarizibility of particle i, and the number of electrons in atom i. Using the value for α_C provided in Ref. [41] we find $\varepsilon_{CC}/k = 41.32\,K$.

For the neopentane micropore fluid, the site-site interactions are strictly intermolecular. The parameters for the C—Me interaction are computed using the Lorentz-Bertholet rules, i.e. $\sigma_{CMe} = 3.565\,Å$ and $\varepsilon_{CMe}/k = 54.54\,K$. The methyl-methyl parameters are those cited above, and the complete neopentane particle structure is defined by the Me—C—Me angle and the C—Me bond length 1.53 Å [21]. This bond length is also employed in the n-pentane simulations and, in addition to the bending and torsional intramolecular interactions described by Equations (15) and (16), methyl and methylene groups in the same molecule which are separated by three groups are subject to the Lennard-Jones (12–6) pairwise interaction.

The alkane/silica potential function is also provided by individual alkane site/oxygen atom LJ(12–6) interactions. The adequacy of this assumption, and the further assumption that the alkane/silicon atom interactions may be neglected, was demonstrated in Ref. [10] for adsorption and diffusion of methane in silica gel. Based on the potential parameters estimated in these earlier studies we obtain the alkane site/oxygen parameters provided in Table I.

In the simulations proper, the LJ(12-6) potential for all pairwise interactions was truncated and shifted as follows

$$\begin{aligned} \Phi_{ij}(r_{ij}) &= \Phi_{ij}^{LJ}(r_{ij}) - \Phi_{ij}^{LJ}(R_c) \quad r_{ij} \leqslant R_c \\ &= 0 \qquad\qquad\qquad\qquad\quad r_{ij} > R_c \end{aligned} \tag{20}$$

where R_c is the cutoff distance and was taken to be equal to 3.5 times the diameter of the interacting sites. The trajectories of the admolecules within the microporous silica

Table I Site-Site Interaction Parameters for Neopentane and n-Pentane Systems

Interacting Sites	[a]ε/k	[b]σ
C—C	41.32	3.207
Me—Me	72	3.923
Me—O	149.96	3.462 (singly bonded oxygen)
	149.96	3.312 (doubly bonded oxygen)
C—Me	54.54	3.565
C—O	113.60	3.104 (singly bonded oxygen)
	113.60	2.954 (doubly bonded oxygen)

[a] ε/k is the well depth parameter in the LJ interaction potential

[b] σ is the effective LJ diameter computed using Lorentz-Bertholet rule $\sigma_{ij} = (\sigma_i + \sigma_j)/2$.

medium were traced using an iterative numerical technique known as RATTLE which incorporates a velocity Verlet finite difference scheme in the original SHAKE algorithm [24]. In this coordinate resetting procedure the external force $\boldsymbol{F}_i$ acting on a molecule is supplemented with an internal force arising primarily due to the existence of constraints (fixed site-site distances in this study). Under these conditions, the Lagrangian equations of motion of the first kind simplify to

$$\begin{aligned} m_i\ddot{\boldsymbol{r}}_i &= \boldsymbol{F}_i + \boldsymbol{C}_i \\ &= -\nabla_i\Phi_i - \sum_{k=1}^{n} \lambda_k \nabla_i \chi_k \quad (i = 1, \ldots, \mathrm{N}) \end{aligned} \tag{21}$$

where $\boldsymbol{C}_i$ is the force contribution due to the constraints, and χ_k is the constraint of a fixed site-site distance, $\boldsymbol{d}_k$, for sites i and j which is given by

$$\chi_k = (\boldsymbol{r}_j(t) - (\boldsymbol{r}_i(t))^2 - d_k^2 = 0 \quad (k = 1, \ldots, n). \tag{22}$$

The total number of constraints is n and λ_k the Lagrangian multiplier for the kth constraint for a molecule with N sites. Equations (21) and (22) constitute 3N + n unknowns corresponding to $\{\boldsymbol{r}(t), \lambda(t)\}$. If the positions and velocities of the sites are known, and if all constraints are satisfied, then at a later time $t = \delta t$ the position vectors $\{\boldsymbol{r}(\delta t)\}$ and the Lagrange multipliers can be uniquely calculated by simultaneously solving the set of 3N + n equations. The solution procedure, which involves the iterative SHAKE algorithm, has been described and reviewed in a number of sources [20–22, 24] to which the reader is referred for details.

To start a given simulation, the alkane particles are initially introduced into the pore space using a straightforward Monte Carlo insertion procedure. Velocities were assigned from the Maxwell-Boltzmann distribution at the appropriate temperature and the system was equilibrated by solving Equations (21) and (22) over a period of time equal to 0.25 ns. This corresponds to 5000 timesteps of magnitude $\Delta t^* = 0.01$ for neopentane and 10,000 timesteps of magnitude $\Delta t^* = 0.005$ for n-pentane where t^* is in units of $l_{\mathrm{SiO}}\sqrt{m_{\mathrm{CH_3}}/\varepsilon_{\mathrm{MeO}}}$. Velocity scaling was employed during this time period and the energy, temperature and velocity distribution were monitored to ensure the system had reached equilibrium prior to computation of the trajectories in the microcanonical ensemble from which the properties described above in section 2.1 were determined. As noted in Table II, the total number of time steps employed was 30,000 for a loading of $N_A = 34$ and 20,000 for $N_A = 90$ and 159.

The alkane studies reported here were conducted at three temperature 225 K, 317 K and 450 K, and the surface coverages cited above are predominantly in the submonolayer region. These conditions are typical of industrial separation processes and, to a lesser extent, heterogeneous catalysis. In addition, the neopentane studies complement the earlier work on SF_6 [11] which was conducted at a single temperature. In Ref. [11] the SF_6 molecule was treated as a structureless Lennard-Jones particle with potential parameters $s = 5.51$ Å and $\varepsilon/k = 200.9$ K. Since the orientationally averaged diameter of the neopentane molecule is 5.78 Å, a comparison between the neopen-

Table II Time Steps Employed in the MD Simulations

T^*	Δt^*		
	0.674	*0.95*	*1.347*
neopentane	0.01	0.01	0.01
n-pentane	0.005	0.005	[a]0.0025

[a] For the maximum loading conditions investigated $\Delta t^* = 0.0015$. Otherwise the given time steps were used for all surface coverages with Δt^* in units of $l_{SiO}\sqrt{(m_{CH_3}/\varepsilon_{MeO})}$ where the Si—O bondlength, $l_{SiO} = 0.162$ nm. All results were evaluated from an average of alteast five different initial configurations for the admolecules for both systems. The total number of timesteps employed was 3×10^4 for $N_A = 34$ and 2×10^4 for the other two particle numbers $N_A = 90$ and 159.

tane/silica simulation results and those reported in Ref. [11] will serve to illustrate the effect of molecular structure on the behavior of rigid particles confined within the microporous silica medium.

3 RESULTS AND DISCUSSION

The discussion which follows has been divided into three sections, (i) equilibrium properties, (ii) dynamical properties, and (iii) diffusion, and in each case the results for neopentane and n-pentane are discussed in turn.

3.1 Equilibrium Properties

If a tetrahedra neopentane molecule is placed on a smooth planar surface this particle would, on average, rest on three of its peripheral methyl groups with the fourth C—CH_3 bond perpendicular to the surface. Since the silica surface is heterogeneous in nature it is of interest to determine to what extent this influences the orientational configuration of the neopentane molecule. Figure 1 provides a schematic view of a neopentane molecule near the silica surface. The angles between the different unit vectors shown in Figure 1, are provided in Table III for the range of conditions investigated in this work. It is interesting to note that the surface configuration is essentially unaffected by both temperature and loading and, as the orientational data in Table III infer, the neopentane molecules near the solid surface tend to assume a configuration similar to that on a flat surface. However, due to the curvature as well as the heterogeneity of the silica microspheres, the particles are tilted in such a way that the three methyl groups on a given particle which are closest to the surface are not at the same distance from the center of the sphere. This observation has a direct bearing on the manner in which the adlayer builds up on the solid surface and will be considered in more detail below.

Selected radial distribution functions at intermediate loading for the center-of-mass (RDFM) and the individual sites (RDFA) of the neopentane particles relative to the

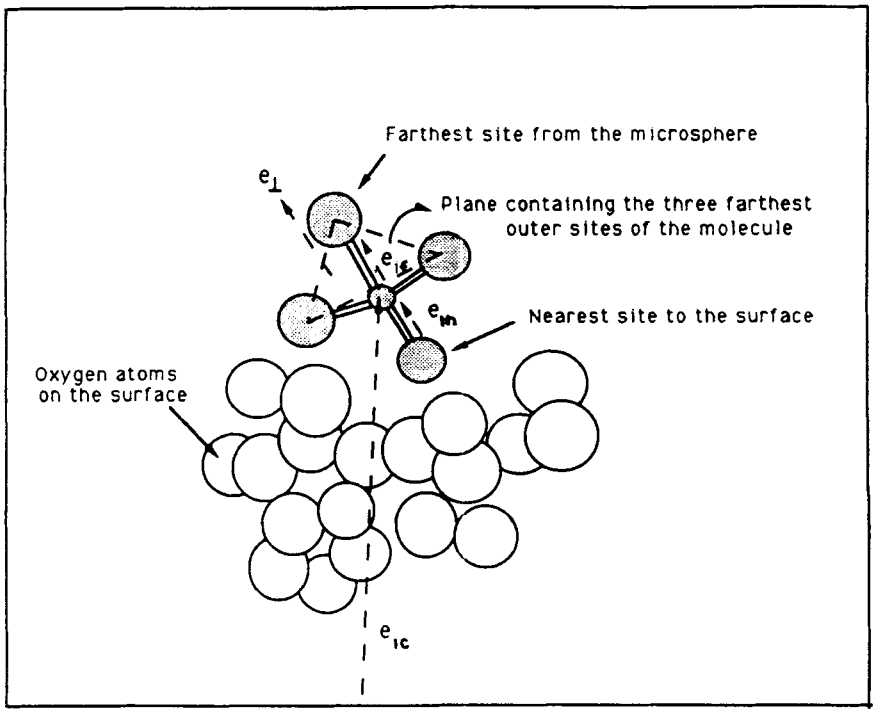

Figure 1 A schematic representation of the neopentane molecule near the atomic surface of microporous silica where the different unit vectors used to define the surface configuration of the particle are shown. The dashed arrows indicate the direction of these unit vectors.

Table III Equilibrium Properties of Neopentane and n-Pentane for a range of loading and temperature conditions.

	$N_A = 34$			$N_A = 90$			$N_A = 159$		
	$T = 225$	$T = 317$	$T = 450$	$T = 225$	$T = 317$	$T = 450$	$T = 225$	$T = 317$	$T = 450$
[a]Ψ	40.0(1)	39.74(8)	39.95(9)	40.69(1)	40.2(1)	40.25(6)	41.16(4)	40.30(6)	40.27(3)
[a]χ	43.39(3)	43.9(1)	43.7(1)	43.4(1)	43.5(1)	43.43(7)	42.91(6)	43.41(8)	43.41(1)
[b]ζ	70.7(2)	72.1(9)	70.1(4)	71.7(9)	70(1)	68.59(5)	69.7(7)	69.0(3)	69.0(0)

[a] These angles determine the surface configuration of a neopentane molecule and were evaluated using Equations (13) and (14).

[b] ζ is employed in an effort to examine the n-pentane conformation near the silica surface. As the value of this angle increases towards 90° the particle is approaching an orientation that is parallel to the solid surface.

center of the silica microspheres are illustrated in Figures 2(a) and 2(b) respectively. The distinction between the RDF's is most clearly demonstrated by the appearance of a series of shallow peaks in the center-of-mass RDF's over the range $13.0 < r^* < 16.0$. This behavior was also observed at other loadings and is primarily caused by the filling of the crevices in the vicinity of the contact points of two adjacent microspheres.

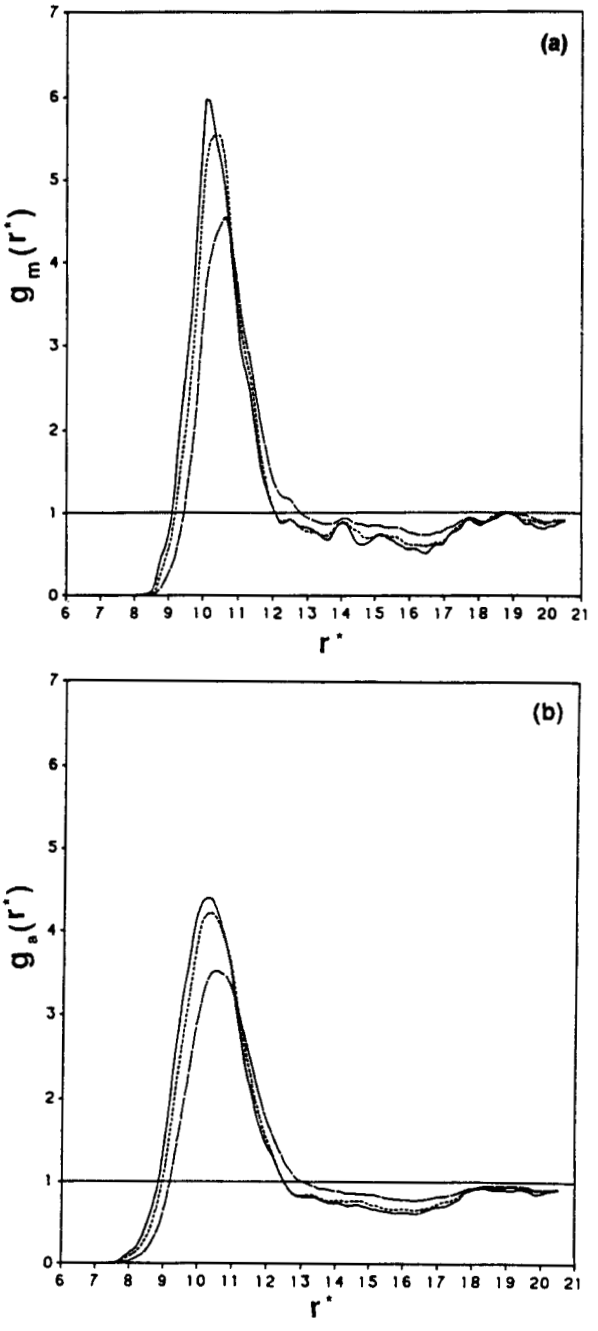

Figure 2 Equilibrium functions for the neopentane system. (a) RDFM- radial distribution of the center of mass of the admolecules, (b) RDFA-radial distribution of the different sites on any individual particle with respect to the silica microsphere centers. (c) Density Profiles for the center of mass distribution. The loading condition in all these functions is $N_A = 90$, and r^* is in units of Si—O bondlength = 0.162 nm. ———— $T = 225$ K, ---------- $T = 317$ K and — — — — $T = 450$ K.

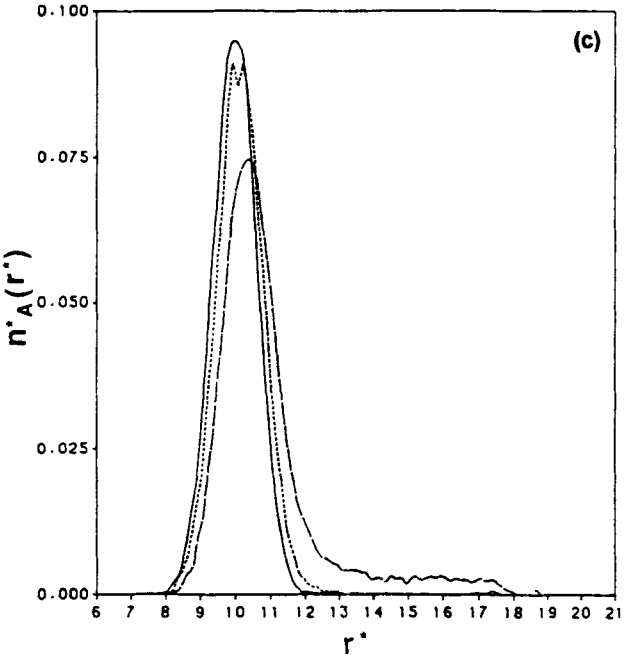

Figure 2 *(Continued.)*

Although a similar effect was observed in the structureless SF_6 particle results reported in Ref. [11], the mechanism involved in the present case is believed to be significantly different. The tilted surface orientation of the neopentane admolecules discussed above enhances the adsorption probability by promoting interlocking of neopentane configurations. Such behavior has also been observed in the bulk liquid phase consisting of tetrahedrally structured particles [43, 44] and is considered to be responsible for the comparatively high packing densities involved in liquid CCl_4 and other fluids composed of tetrahedral molecules. In the present case the interlocking configurations enhance the preferential accumulation of the adsorbate as small clusters near the contact points of the silica particles.

The neopentane density profiles provided in Figure 2(c) demonstrate another feature common to all of the simulations conducted here. As the temperature is increased the adlayer becomes more diffuse as expected. However, in contrast to the comparatively small change involved in changing the temperature from 225 K to 317 K at a given loading, a similar change in temperature to 450 K results in a much broader density profile with a large proportion of the neopentane particles distributed within the pore volume. Although the neopentane molecular model employed here is not a exact representation of the real fluid it is of interest to note that the highest temperature employed in this work is above the critical temperature of neopentane. We believe the diffuse structure of the density profile at 450 K reflects a corresponding supercritical state in the model fluid and later in section 3.3 we will show that the critical transition

implied by the profiles in Figure 2(c) also seriously influences the temperature dependent behavior of the transport properties of the adsorbed fluid.

The surface configuration of the n-pentane admolecules are, in part, characterized by the angle ζ as defined in Equation (14) and the simulation results for this quantity are provided in Table III. From this table it is seen that an increase in surface coverage tends to decrease the value of ζ which implies that the major axis of the particle is, on average, less likely to be parallel to the solid surface. The influence of temperature, however, is not as straightforward as indicated by the results for $N_A = 34$. Contrary to the gradual decrease observed at higher coverages there appears to be preferential orientation parallel to the surface at $T = 317$ K. At low coverages admolecule/admolecule interactions are negligible and therefore at low temperatures the n-pentane particles are able to penetrate the silica microspheres via microcavities present on the heterogeneous surface. However, with increasing temperature the occupancy of these low potential energy cavities is depleted with the result that at intermediate temperatures the admolecules initially assume orientations parallel to the solid surface and with further increase in T the thermal energy of the particles induces randomization of the adsorbed layer.

The above observations are further supported by the simulation results for the RDFM's, RDFA's and density profiles. These results are illustrated in Figure 3 at the intermediate loading $N_A = 90$ and over the range of temperatures 225 K to 450 K. At low temperatures the n-pentane particles readily penetrate the silica microspheres as evidenced by the weak shoulder in the RDF's and in the density profile at low T. Although not shown here, this shoulder is much stronger for $N_A = 34$ (peaking, for example, at 0.55 for the RDFM) while it is essentially nonexistent for a loading of $N_A = 159$. As the temperature is increased the shoulder disappears and the n-pentane particles are, on average, located further from the surface. This is also demonstrated by the shift in the dominant peak position with increasing temperature.

In comparing the RDF's and density profiles for neopentane and n-pentane we observe three distinct differences. Firstly, at low to moderate temperatures the LJ sites of the linear n-pentane molecules penetrate nearly 2 Å further into the silica microspheres. Secondly, the shallow peak in the RDFM's for n-pentane at $r^* = 13.0$ is closer to the silica microsphere than the corresponding peak for neopentane. And thirdly, the distribution functions and profiles for n-pentane are more sharply peaked. All of these observations are directly related to the elongated and flexible structure of the n-pentane particles in contrast to the compact and rigid structure of the neopentane molecules. Due to the closer proximity of the n-pentane particles to the silica surface, the adsorptive interactions for this component are stronger and, as will be shown later, the diffusive behavior is also significantly affected.

The influence of the silica surface on the internal conformations of the n-pentane particles is clearly demonstrated in Figure 4. In Figure 4(a) the bond angle distributions for $N_A = 34$ are plotted for each of the temperatures investigated in this work. Also shown in this figure is the bond angle distribution for the ideal gas state at the intermediate temperature 317 K and this distribution is seen to be much narrower than the corresponding one in the presence of the solid surface. We believe the extensive broadening of the distribution experienced by the adsorbed fluid is due primarily to near-commensurate interactions between adjacent triplets of methyl and methylene

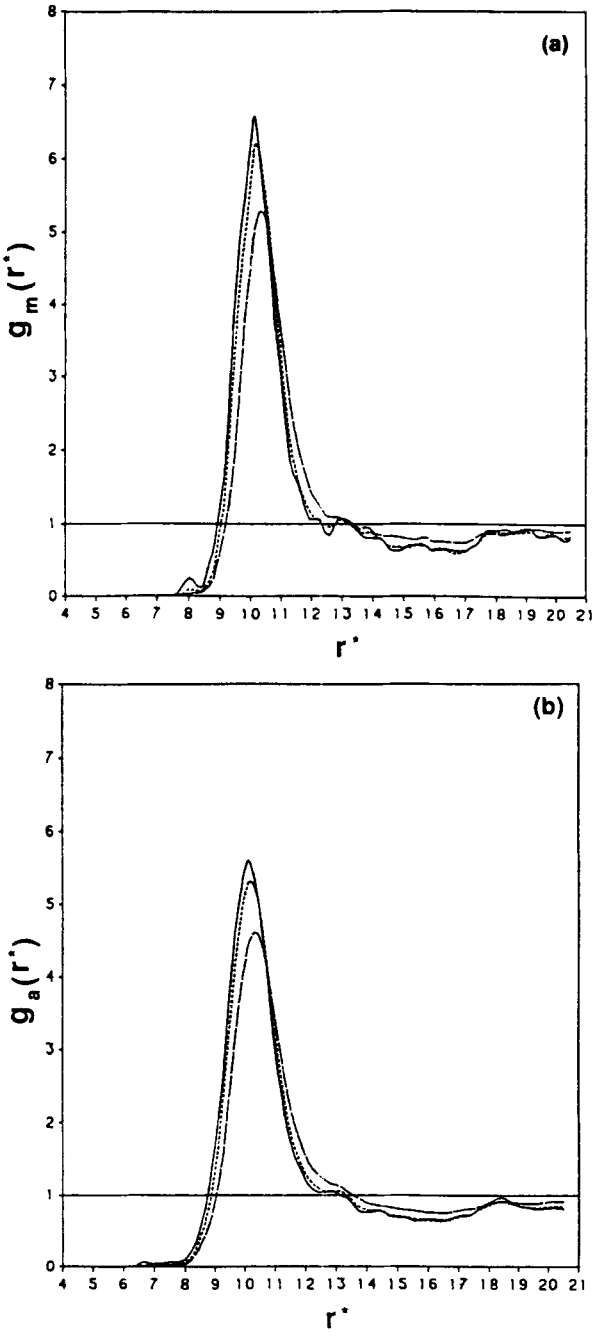

Figure 3 Equilibrium functions for the n-pentane system. (a) RDFM-radial distribution of the center of mass of the admolecules, (b) RDFA-radial distribution of the different sites on any individual particle with respect to the silica microsphere centers. (c) Density Profiles for the center of mass distribution. The loading condition in all these functions is $N_A = 90$, and r^* is in units of Si—O bondlength = 0.162 nm. ———— $T = 225$ K, ---------- $T = 317$ K and — — — — $T = 450$ K.

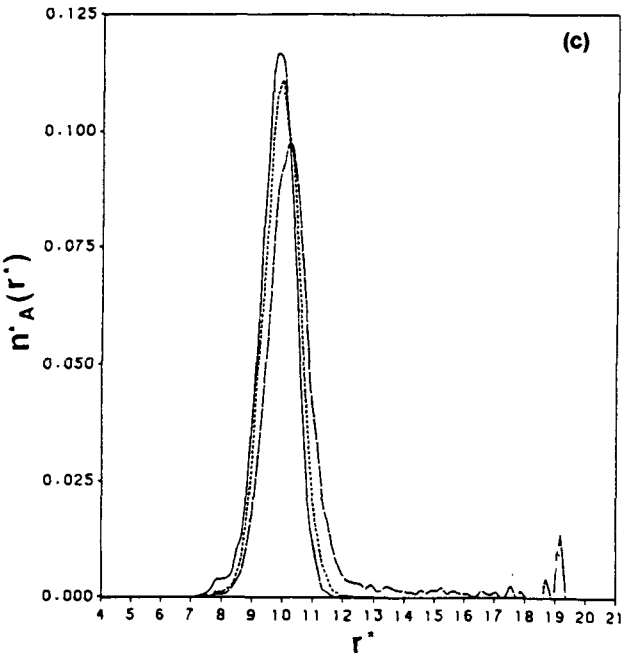

Figure 3 *(Continued.)*

sites on the n-pentane molecule and oxygen triplets on the silica surface. For the model systems under consideration here it is worth noting the following characteristic length scales: in the n-pentane molecule the intersite distance is 1.53 Å and the average distance between next-to-nearest neighbor sites is 2.495 Å; the local structure of the model silica surface involves edgewise interconnected triangles of oxygen atoms the sides of which are 2.6 Å in length and the centers of which are, on average, a minimum distance of 0.75 Å from their respective edges [11]. If it is assumed that the potential minima for adsorption of the methyl and/or methylene sites are located at the centers of the triangles formed by the oxygen atoms then it is not unreasonable to expect the n-pentane molecules to be stretched out over the silica surface with the LJ sites occupying the potential minima of five adjacent oxygen triplets. If three adjacent oxygen triplets are coplanar this could result in a bond angle stretching of approximately 7°. Bond angle compression also occurs due to the irregular structure of the solid surface and this coupled with partial stretching leads to the broadening in the adsorbed phase distribution shown in Figure 4(a). As the temperature is raised the vibrational kinetic energy of the adsorbed n-pentane particles increases with a consequent increase in the width of the bond angle distribution. It is tempting to speculate that the severe distortion in this distribution, and particularly the large proportion of strained bonds at high temperatues, may provide a low energy pathway for charge transfer and hence the formation of carbonium ions which are usually considered to be the prevalent intermediates in heterogeneous catalytic cracking reactions.

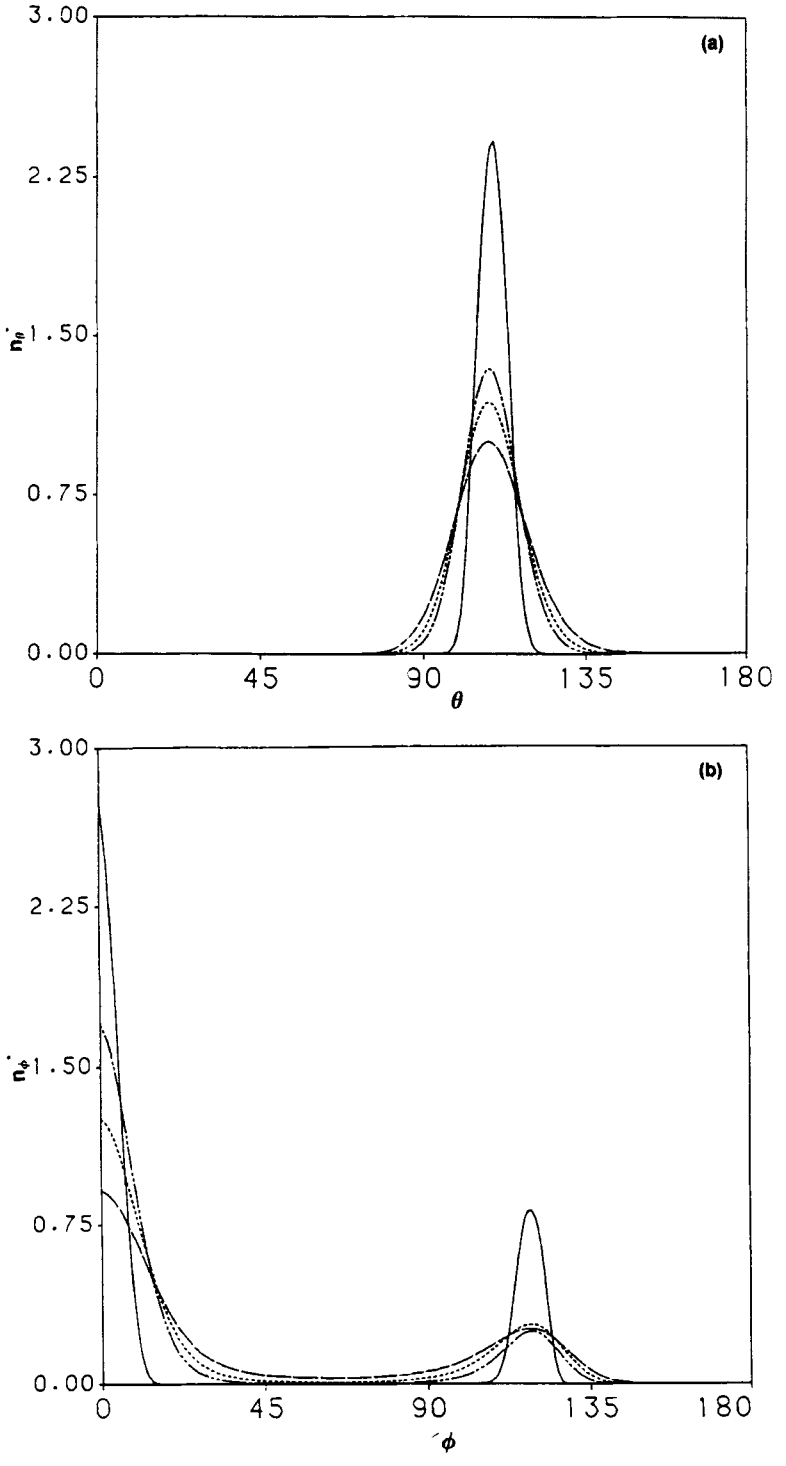

Figure 4 The internal conformations of the n-pentane molecule are characterized by its bond angles and dihedral angles whose distributions are shown in this figure. (a) Bond angle distribution and (b) Dihedral angle distribution for $N_A = 34$ loading condition. Gaseous state, ———— $T = 225$ K, ---------- $T = 317$ K and — — — — $T = 450$ K.

The extended structure of the n-pentane particles in the adsorbed phase is also clearly demonstrated by the results obtained for the dihedral angle distribution shown in Figure 4(b). The adsorbed n-pentane molecules are predominantly in the TT (trans-trans) conformational state at low temperatures in comparison with the gas phase and this is further emphasized by the entries in Table IV. In this table we report the ratio of trans-to-gauche conformations for the complete range of loading and temperature conditions involved in this work. The much higher trans-gauche ratio for the admolecules in contrast to the ideal gas (2:1) is indicative of the stretched conformations which predominate in the adsorbed phase. This effect is also evident from the results for the end-to-end distance and the radius of gyration of the n-pentane particles. As the temperature is increased the particles become more compact as illustrated by the drop in $\langle r \rangle$ and the ratio $T/G^{\pm}$ and from Figure 4(b) it is of interest to note that the underlying reason for this is due primarily to a sharp increase in the number of intermediate conformational states at the expense of a drop in the number of trans conformations.

3.2 *Dynamical Behavior*

The normalized tracer velocity autocorrelation function (VACF)

$$C_{i^*i^*}(t^*) = \langle \boldsymbol{v}_i(0) \cdot \boldsymbol{v}_i(t) \rangle / \langle v_i^2(0) \rangle \tag{23}$$

Table IV Equilibrium Properties of Neopentane and n-Pentane for a range of loading and temperature conditions.

	$N_A = 34$			$N_A = 90$			$N_A = 159$		
	$T = 225$	$T = 317$	$T = 450$	$T = 225$	$T = 317$	$T = 450$	$T = 225$	$T = 317$	$T = 450$
[a]$\langle \Phi_{Am} \rangle 10^{-1}$	−2.7(1)	−2.4(1)	−2.09(1)	−2.60(2)	−2.29(2)	−1.73(4)	−2.37(1)	−2.04(1)	−1.61(1)
[a]$\langle \Phi_{AA} \rangle$	−0.56(3)	−0.55(3)	−0.42(2)	−1.85(6)	−1.53(3)	−1.17(3)	−2.92(5)	−2.58(1)	−2.11(1)
[b]$\langle \Phi_{Am} \rangle 10^{-1}$	−3.9(1)	−3.7(3)	−3.2(5)	−3.59(3)	−3.20(3)	−2.60(1)	−3.22(5)	2.8(2)	−2.30(1)
[b]$\langle \Phi_{AA} \rangle$	−1.3(2)	−1.2(1)	−1.10(4)	−2.9(2)	−2.58(9)	−2.05(5)	−4.67(3)	4.3(1)	−3.3(1)
[c]$\langle \Phi_{\phi} \rangle$	−1.49(6)	2.0(1)	2.84(4)	1.36(3)	1.99(2)	2.79(2)	1.457(5)	2.079(9)	2.821(7)
[c]$\langle \Phi_{\theta} \rangle$	−0.80(3)	1.08(4)	1.50(2)	0.765(8)	1.046(8)	1.483(8)	0.788(3)	1.078(6)	1.50(1)
[d]$\langle T \rangle$	234(10)	324(13)	461(7)	228(2)	313(3)	457(7)	234(2)	327(1)	457(3)
[e]$\langle r \rangle$	2.879(6)	2.833(3)	2.788(7)	2.903(7)	2.835(4)	2.798(5)	2.881(2)	2.829(1)	2.796(2)
[e]$\langle S \rangle$	1.079(1)	1.0693(6)	1.060(1)	1.084(2)	1.0699(7)	1.062(1)	1.0794(4)	1.0684(2)	1.062(4)
[f]$T/G^{\pm}$	3.12	2.43	1.97	4.29	2.78	2.18	3.65	2.32	2.14

[a]$\langle \Phi_{Am} \rangle$ and $\langle \Phi_{AA} \rangle$ are the average potential energies per molecule in units of ε_{MeO} for admolecule/solid and admolecule/admolecule interactions, respectively, in the neopentane system.

[b]$\langle \Phi_{Am} \rangle$ and $\langle \Phi_{AA} \rangle$ are the average potential energies per molecule in units of ε_{MeO} for admolecule/solid and admolecule/admolecule interactions, respectively, in the n-pentane system.

[c]$\langle \Phi_{\phi} \rangle$ and $\langle \Phi_{\theta} \rangle$ are the average potential energies per angle for dihedral and bond angles contributions, respectively, in units of ε_{MeO}.

[d]$\langle T \rangle$ is the average temperature of the n-pentane system computed from the kinetic energy of the center of mass of the particle.

[e]$\langle r \rangle$ and $\langle S \rangle$ are the average end-to-end distance and radius of gyration in units of l_{SiO}.

[f]$T/G^{\pm}$ is the ratio of the trans- to gauche conformations calculated from the dihedral angle distributions in the n-pentane system.

and the total adsorbate velocity autocorrelation function (TVACF)

$$C_{AA}(t^*) = \langle \boldsymbol{u}_0(0) \cdot \boldsymbol{u}_0(t) \rangle / \langle u_0^2(0) \rangle \tag{24}$$

for neopentane are presented in Figures 5 and 6. At each of the temperatures investigated these autocorrelation functions appear to be only weakly dependent on loading and this is in sharp contrast to the results reported earlier for a structureless Lennard-

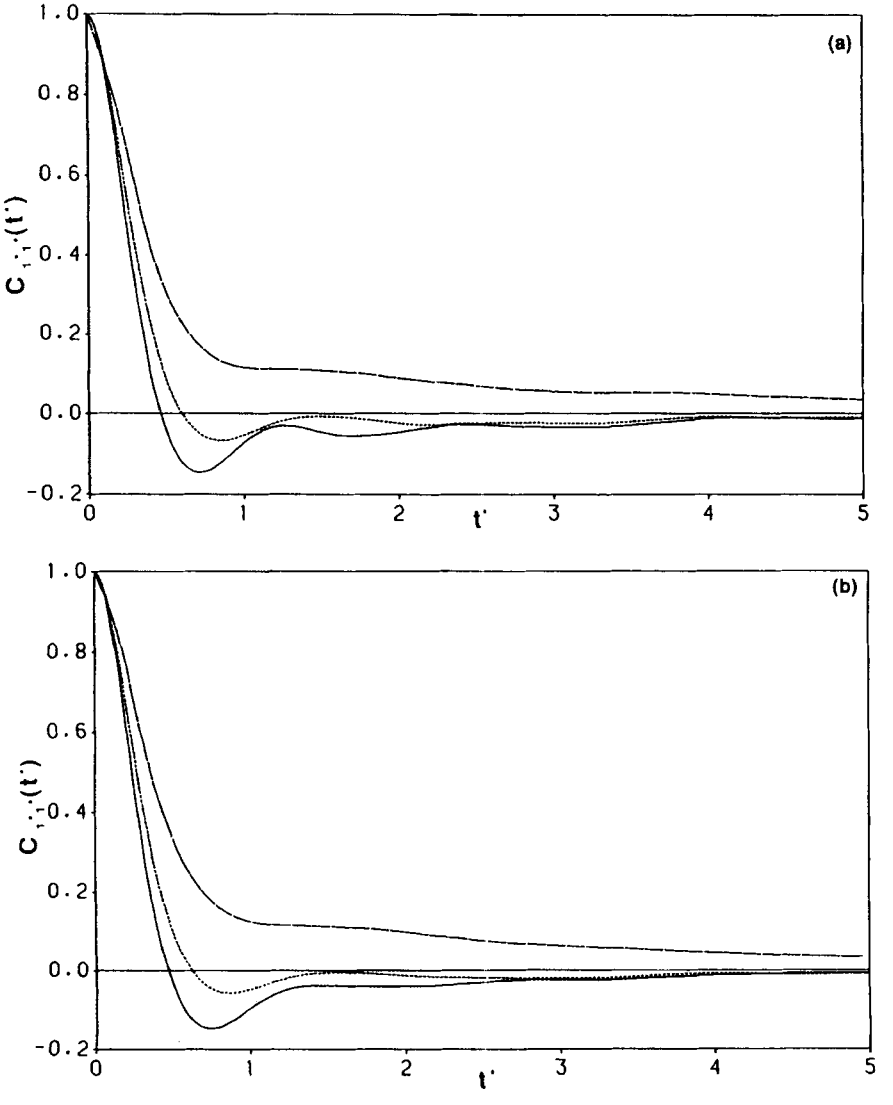

Figure 5 Tracer velocity autocorrelation functions for different temperatures and loading conditions for the neopentane system. (a) $N_A = 34$, (b) $N_A = 90$ and (c) $N_A = 159$. ——— $T = 225$ K, ---------- $T = 317$ K and — — — — $T = 450$ K.

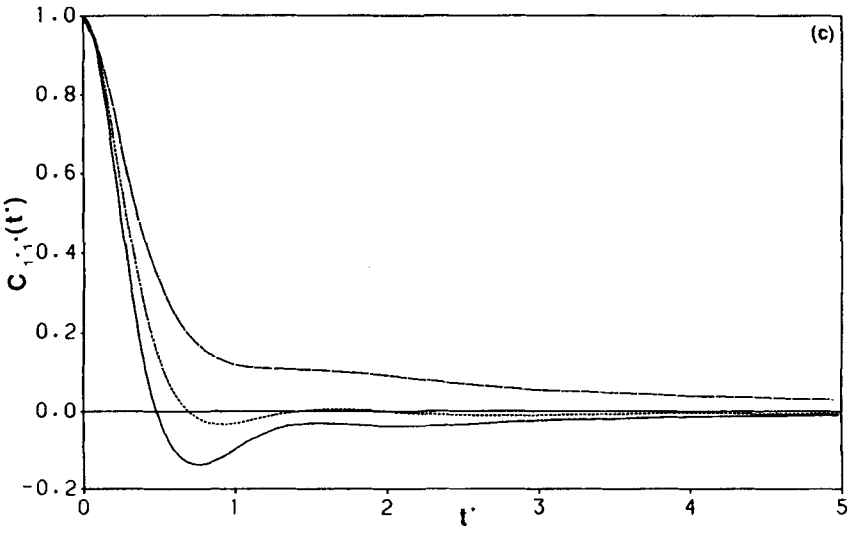

Figure 5 *(Continued.)*

Jones SF_6 fluid [11]. A comparison between these two systems may be made when it is noted that the orientationally averaged interaction between two model neopentane particles is closely approximated by a Lennard-Jones 12-6 potential function with admolecule parameters $\varepsilon_{AA}/k = 334\,\text{K}$ $\sigma = 5.78\,\text{Å}$. At low loadings the decay of the VACF is primarily determined by admolecule/solid interactions and we may therefore consider the reduced temperature $T^* = kT/\varepsilon_{AO}$ as a basis for intercomparison of both systems. In Ref. [11] a single reduced temperature $T^* = 0.762$ was investigated and in the present case, using the Lorentz-Bertholet rule $\varepsilon_{AO} = (\varepsilon_{AA}\varepsilon_{OO})^{1/2}$ for the orientationally averaged neopentane particles, we find that the conditions which most closely relate to the SF_6/silica system studied in Ref. [11] correspond to $T = 225\,\text{K}$ i.e. $T^* = 0.697$. In the SF_6 system at $T^* = 0.762$ the first minimum in the tracer VACF experienced a significant shift upward to the right (to longer times) when the loading was increased from $N_A = 34$ to 159 (between one fifteenth and one third of a monolayer). In Ref. [11] this behavior was associated with screening of high energy sites by particles preadsorbed on the heterogeneous solid surface. This was ultimately responsible for a SF_6 diffusion coefficient which was found to increase rapidly with surface coverage. We still expect surface screening to be present in the neopentane system however it is clear that the influence of surface heterogeneity is weaker in the present case. This is also suggested by the much shallower backscattering minima in both the VACF's and the TVACF's for neopentane in comparison with the SF_6 autocorrelation functions under similar conditions. Although there are significant quantitative differences between the SF_6 results reported in Ref. [11] and the neopentane results under consideration here, these data are in good qualitative agreement in a number of ways. The trends in the first and second backscattering minima in the TVACF's shown in Figure 6 are similar to those observed in Ref. [11] for the SF_6/silica system. The origin of this behavior was shown in Ref. [11] to be due to the increasing influence of momentum cross-correlations within the pore fluid with increased loading.

Selected time correlation functions characterizing the rotational dynamics of the neopentane admolecules at low loadings are provided in Figure 7 and 8. The normalized angular momentum correlation functions shown in Figure 7 exhibit trends expected for severely hindered rotation, particularly at the lowest temperature investigated, and this suggests that the tumbling motion characteristic of bulk fluids of rigid tetrahedral particles is of minor importance in the presence of a solid surface. This conclusion is further supported by the results shown in Figure 8 for the orientational

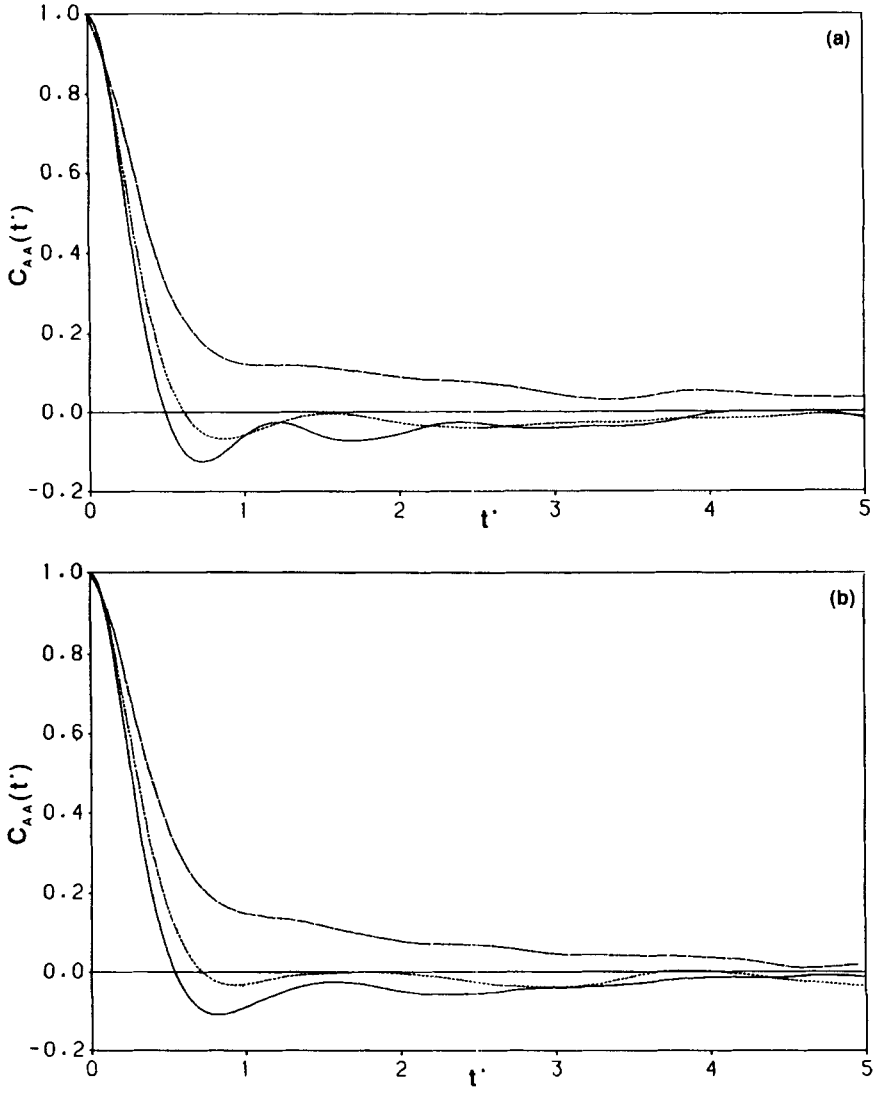

Figure 6 Velocity autocorrelation functions for the overall center of mass of the neopentane fluid at different temperatures and surface coverages. (a) $N_A = 34$, (b) $N_A = 90$ and (c) $N_A = 159$. ———— $T = 225$ K, ---------- $T = 317$ K and — — — — $T = 450$ K.

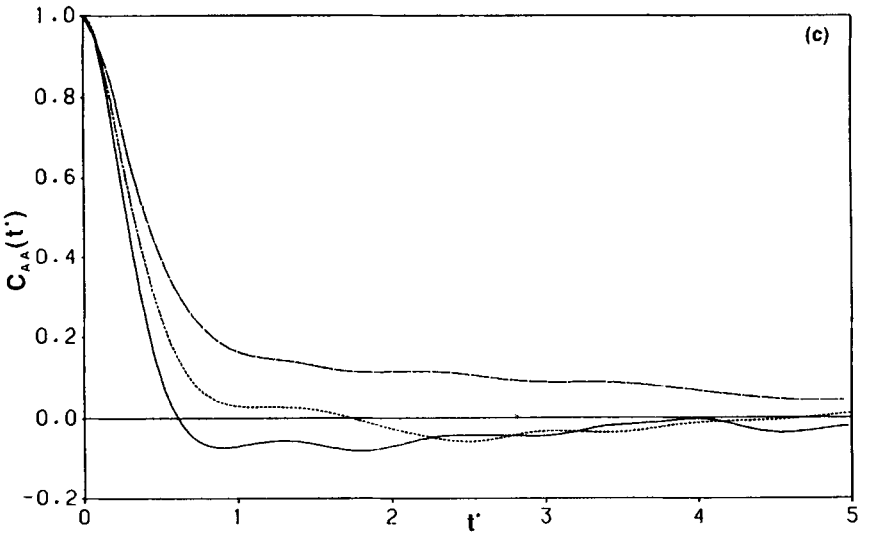

Figure 6 *(Continued.)*

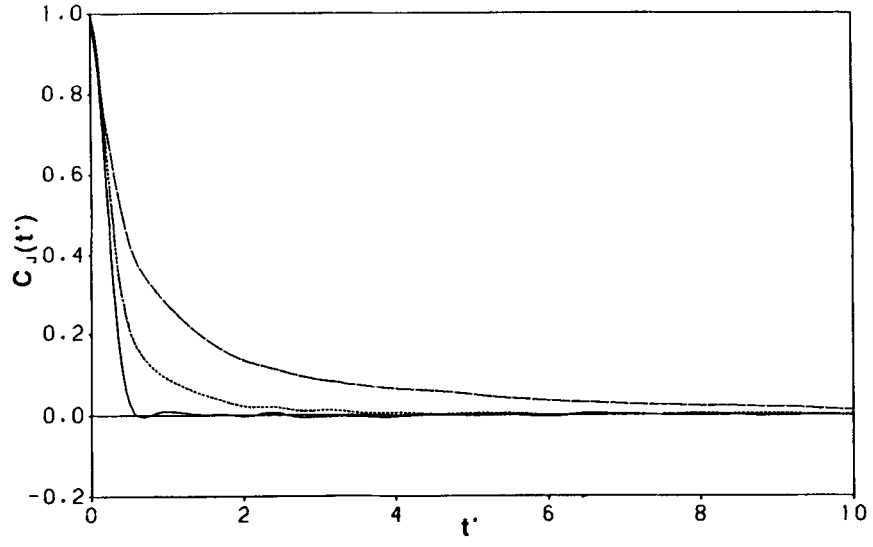

Figure 7 The angular momentum autocorrelation function for the neopentane system over the range of temperature conditions examined for $N_A = 34$ case. ———— $T = 225$ K, ---------- $T = 317$ K and — — — — $T = 450$ K.

correlation functions P_1 and P_2 defined in Equations (6a) and (6b). After an initial rapid decay over a short period of time both of these functions subsequently relax very slowly with time. On close inspection of the complete set of simulation results for P_1 and P_2 over the time range $5.0 < t^* < 40$ we in fact find that the long time tails are well

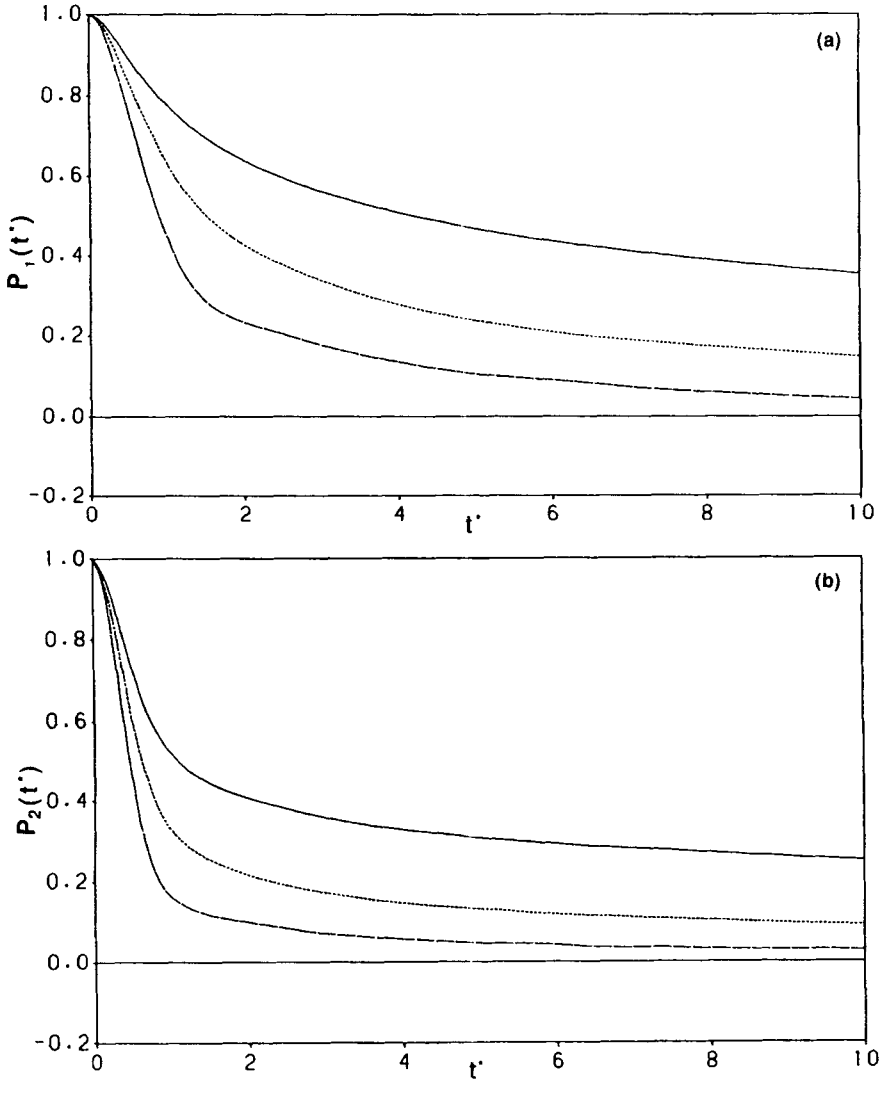

Figure 8 The orientational correlation functions for the neopentane fluid as a function of temperature for $N_A = 34$ loading condition. ——— $T = 225$ K, ---------- $T = 317$ K and — — — — $T = 450$ K.

described by the simple power law

$$\lim_{t^* \to \infty} P_n(t^*) = \frac{A}{t^{*b}} \tag{25}$$

with b essentially equal to 1.0 for all conditions. This result is in sharp contrast to the behavior expected if Brownian motion is assumed to govern the rotational dynamics of

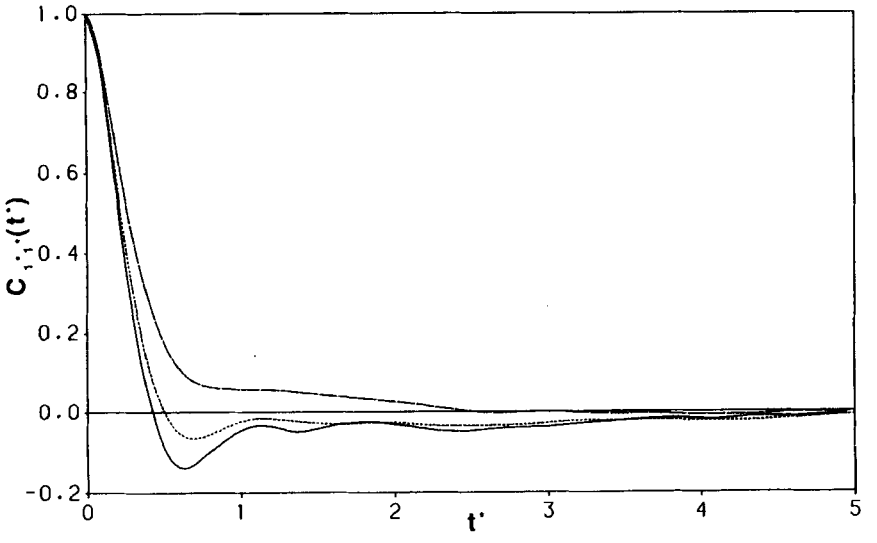

Figure 9 Tracer velocity autocorrelation functions for different temperatures at $N_A = 34$ for the n-pentane system. ——— $T = 225$ K, ---------- $T = 317$ K and — — — — $T = 450$ K.

the particles. In the latter case the correlation functions P_1 and P_2 are predicted to decay exponentially according to

$$P_n = \exp(-n(n+1)D_r t) \tag{26}$$

where D_r is the rotational diffusion coefficient. If we integrate this expression from $t = 0 \rightarrow \infty$ the simple result $1/(n(n+1)D_r)$ is obtained, i.e. the integral is finite and inversely proportional to D_r. The simulation results, however, imply an inverse t^* decay at long times which in turn suggests that the integral of P_n is ill-defined and rotational diffusion (at least in the Brownian sense) is nonexistent. Although the rotational diffusion coefficient is indeed small it is not zero and the above result must cast some doubt on the assumption that reliable estimates of D_r may be extracted from experimental infrared (P_1) and Raman (P_2) spectra of adsorbed species.

The dynamical behavior of the center-of-mass of the n-pentane particles was generally found to be similar to that of neopentane and this may be seen by comparing the VACF's at low loadings shown in Figure 9 with the corresponding results for neopentane provided in Figure 5(a). A number of very important differences exist however, both at high temperatures, where it is observed that the VACF's for n-pentane decay to zero much more rapidly than in the case of neopentane, and at low temperatures where this rapid decay is coupled with a significant shift in the minima in the VACF's to shorter times. Both of these observations are intimately related to the flexibility of the n-pentane particles and the manner in which the intramolecular conformational transitions are influenced by temperature. This is most readily demonstrated by considering the functions ρ_1 and ρ_2 (as defined in Equations (10) and (11))

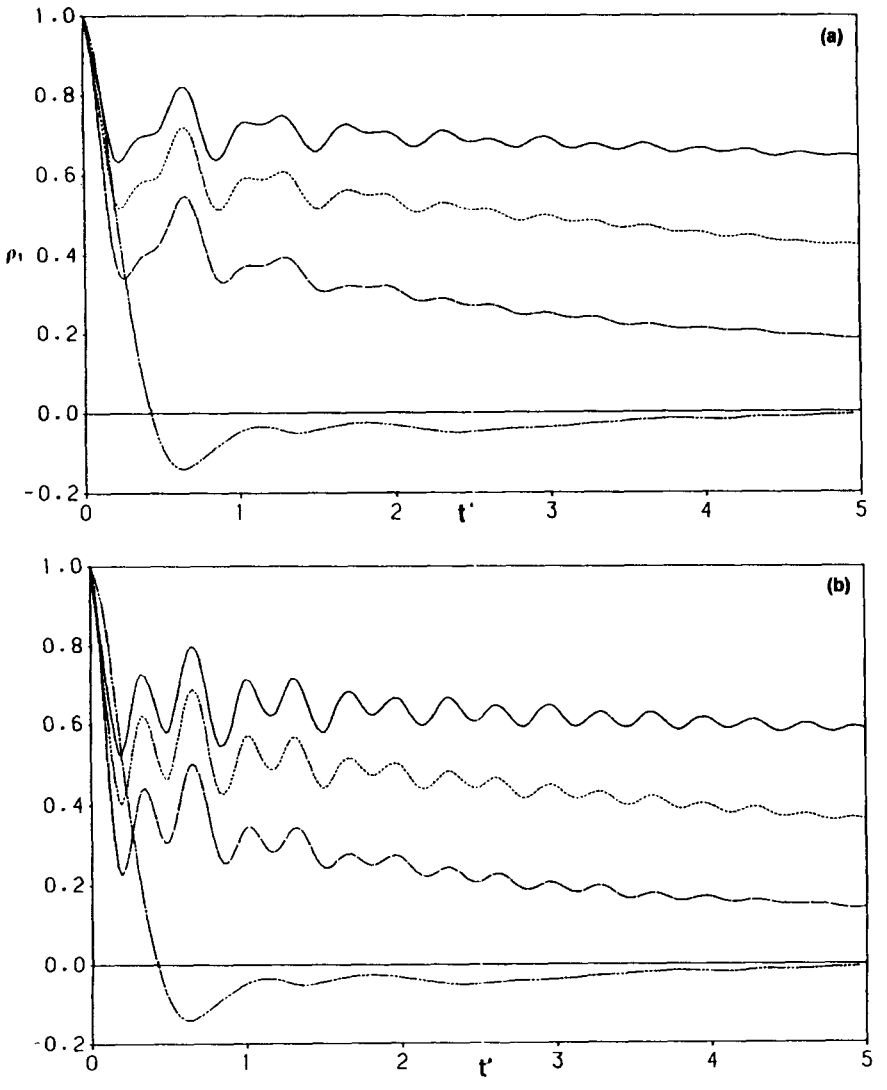

Figure 10 The relaxation mechanisms of the n-pentane molecule near the solid surface are examined by two functions ρ_1 and ρ_2 given in Equations (10) and (11) for $N_A = 34$ loading case. ——— $T = 225$ K, ---------- $T = 317$ K and — — — — $T = 450$ K. VACF for the $N_A = 34$ at $T = 225$ K.

which are plotted in Figure 10 for the lowest loading investigated. Results obtained for these functions at other loadings were quantitatively similar indicating that the internal motion of the n-pentane particles is primarily a function of temperature. The low temperature VACF for n-pentane is also reproduced in Figure 10 and it is observed that the positions of the local maxima in both ρ_1 and ρ_2 closely correspond to the locations of the minima in the VACF. The pulsations exhibited by ρ_1 and ρ_2 arise due to bond angle vibrations and the very slow relaxation of

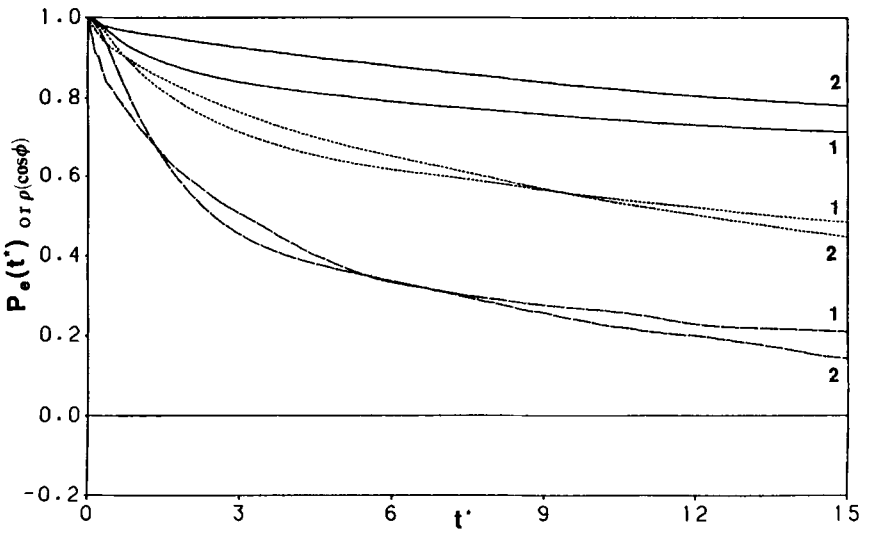

Figure 11 The dihedral angle relaxation and reorientation of the end-to-end vector are shown in this figure where 1: P_e- end-to-end vector decorrelation function and 2: $\rho(\cos\phi)$-dihedral angle relaxation function for $N_A = 34$ loading condition. ——— $T = 225$ K, ---------- $T = 317$ K and — — — — $T = 450$ K.

these functions is believed to be due to a cooperative motion generated between these vibrations and torsional rotations within the n-pentane particles. This cooperative effect, which attempts to maintain a fixed molecular end-to-end distance (or radius of gyration) in the presence of the silica surface, give rise to crankshaft motion

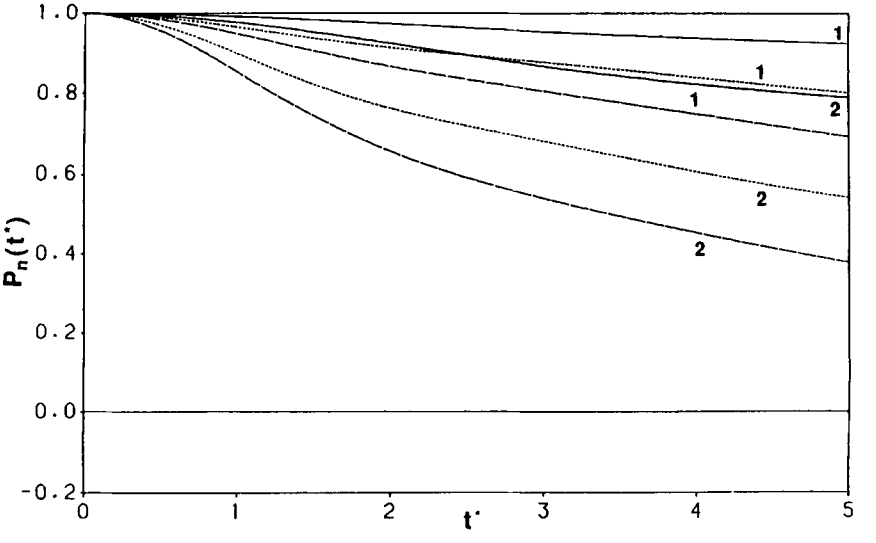

Figure 12 The orientation correlation functions for the n-pentane fluid as a function of temperature for $N_A = 34$ case where 1: P_1 and 2: P_2 for the unit vector along the outermost bond. ——— $T = 225$ K, ---------- $T = 317$ K and — — — — $T = 450$ K.

of the n-pentane molecules and this is believed to be the principal mechanism for diffusion in the adlayer.

As the temperature is increased the frequency of intramolecular dihedral rotations increases. This has a direct effect on the center-of-mass velocities of the n-pentane particles which decorrelate more rapidly than for neopentane under similar conditions. The increased rate of relaxation of the torsional modes of the admolecules with increasing temperature is illustrated in Figure 11 where the correlation function $\rho(\cos\phi)$ defined in Equation (9) is plotted for the range of temperatures investigated at low loading. Also shown in this figure is the end-to-end vector correlation function which was determined using Equation (6a) with $\boldsymbol{u}$ defined as the unit vector directed along the line connecting the first and last sites on a given molecule. The near agreement in the decay rates of both P_e and $\rho(\cos\phi)$ demonstrates that it is the increasing freedom of movement experienced by the molecule as a whole as the temperature is increased which is the underlying reason for the rapid increase in the rate of decay of $\rho(\cos\phi)$ at higher temperatures.

The increase in the reorientational mobility of the n-pentane particles as the temperature is increased is also reflected in the correlation functions P_1 and P_2 shown in Figure 12. The unit vector $\boldsymbol{u}$ in this case is directed along the outermost bonds of the particles and because only a single bond is considered in contrast to the entire molecule in the case of P_e, the functions P_1 and P_2 decay more slowly with time. The very slow relaxation of P_1 at low temperature is believed to be due in part to partial anchoring of the chain either in microcrevices as indicated by the RDFA for n-pentane at $T = 225$ K shown in Figure 3 or on commensurate potential minima on the solid surface. Internal rotation about this anchored end bond would not necessarily require any significant variations in the intramolecular dihedral angles (as implied also in Figure 11) but would require an activated state for molecular diffusion of the center-of-mass to correspond with three of the LJ sites (one methyl and two methylene sites) undergoing a simultaneous jump from a set of three potential minima to another set of three potential minima on the silica surface. This is one possible mode of crankshaft motion for the n-pentane molecules which would result in a net displacement of the center-of-mass of the particles of approximately 0.15 nm. It is noteworthy that the time taken for the center-of-mass of the admolecules to move this distance also closely corresponds the time at which the low temperature VACF's have decayed to zero (a reduced time of approximately 7.0). As the temperature is increased the possible influence of anchoring is reduced and global rotations of the molecules occur with greater frequency.

3.3 *Diffusion*

The VACF's and TVACF's determined in these studies at low-to-moderate temperatures were generally found to be characterized by a long-time tail described by a power law decay of the form

$$\lim_{t^*\to\infty} C_{ii}(t^*) = -\frac{\alpha_p}{t^{*\beta}} \tag{27}$$

Table V The diffusion coefficients as a function of temperature and surface coverage.

	$N_A = 34$			$N_A = 90$			$N_A = 159$		
	$T = 225$	$T = 317$	$T = 450$	$T = 225$	$T = 317$	$T = 450$	$T = 225$	$T = 317$	$T = 450$
$^aD^*_{1\cdot1\cdot}(neo)$	0.014(2)	0.066(4)	0.44(4)	0.014(3)	0.075(6)	0.5(6)	0.0208(7)	0.109(7)	0.504(6)
$^aD^*_{1\cdot1\cdot}(n)$	0.010(2)	0.032(4)	0.22(2)	0.013(2)	0.039(2)	0.33(3)	0.0207(2)	0.088(7)	0.44(4)
$^aD^*_{AA}(neo)$	0.020(2)	0.07(1)	0.47(8)	0.021(6)	0.085(8)	0.48(7)	0.032(2)	0.124(8)	0.53(4)
$^aD^*_{AA}(n)$	0.010(4)	0.035(5)	0.22(3)	0.013(3)	0.07(1)	0.7(1)	0.032(2)	0.11(2)	0.7(1)
$^bD^*_r(neo)$	0.91(7)	2.59(2)	9.0(7)	0.91(6)	1.96(4)	9.4(7)	1.06(2)	2.59(4)	8.3(3)
$^bD^*_r(n)$	0.39(5)	1.2(1)	5.0(4)	0.49(3)	1.50(6)	7.7(7)	0.5759(9)	1.73(5)	10(2)

(*neo*) and (*n*) correspond to quantities in the neopentane and n-pentane systems, respectively.

[a] Diffusivities are in reduced units of $l_{SiO}\sqrt{(m_{CH_2}/\varepsilon_{MeO})}$.

[b] D_r^* is the rotational diffusion coefficient in reduced units of $\varepsilon_{MeO} l_{SiO}\sqrt{(m_{CH_2}/\varepsilon_{MeO})}$.

where α_p and β are the power-law parameters. Although the tails of the correlation functions themselves had substantial statistical noise for reliable fits of the above equation, it was possible to estimate these parameters with reasonable accuracy using the time dependent diffusion coefficients obtained from finite time integration of the

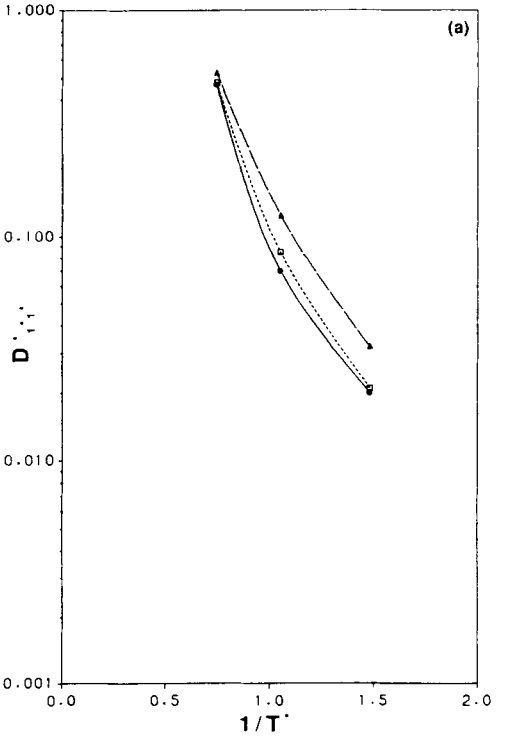

Figure 13 Diffusion coefficients for the neopentane system as a function of $1/T^*$ for the different loading conditions examined in this work. ● $N_A = 34$, □ $N_A = 90$ and △$N_A = 159$. (a) Tracer diffusion coefficients and (b) Overall diffusion coefficient.

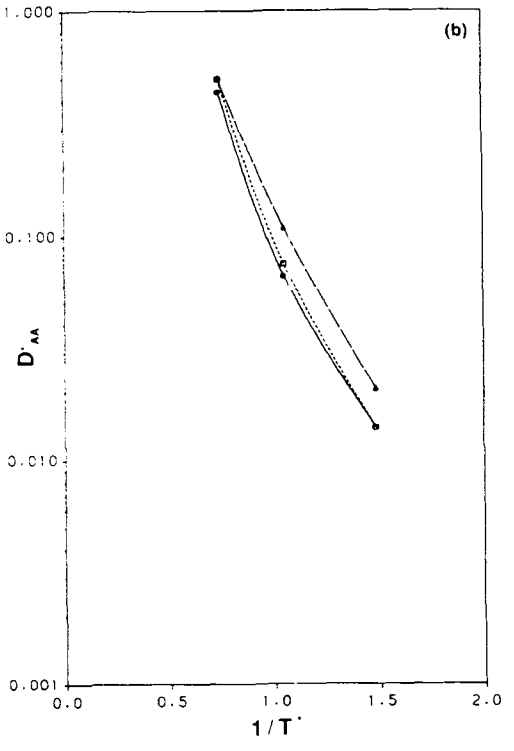

Figure 13 *(Continued.)*

VACF's and TVACF's i.e.

$$\lim_{t^* \to \infty} D_{ii}^*(t^*) = D_{ii}^*(t_0^*) + \frac{\alpha_P}{3(\beta - 1)}[t^{*(1-\beta)} - t_0^{*(1-\beta)}] \tag{28}$$

where t_0^* is a specific time for which the diffusivity is known. It was found that for those runs in which values for β could be obtained these estimates were consistent with the value of 2.5 for Lorentz gases [45–50]. This is not unexpected for submonolayer coverages and the 2.5 power law was therefore used to extrapolate the finite time data for the diffusion coefficients to infinite time to obtain the results provided in Table V.

Figures 13 and 14 illustrate $D_{1\cdot 1}^*$ and D_{AA}^* as functions of $1/T^*$ for neopentane and n-pentane, respectively, over the range of surface coverages investigated. Although these results are only qualitatively described by the Arrhenius form

$$D_{ii}^* = D_0 \exp(-E_t/RT) \tag{29}$$

where D_0 is a constant assumed to be independent of temperature and E_t is the activation energy for diffusion, it is possible to obtain estimates for E_t for comparative

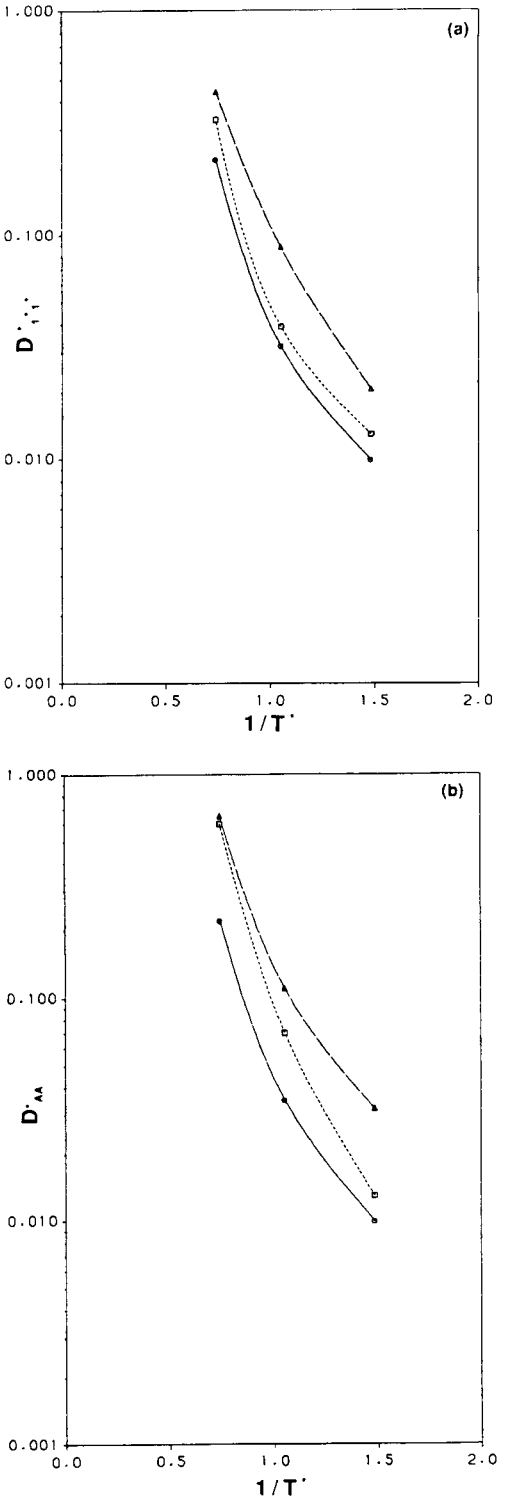

Figure 14 Diffusion coefficients for the n-pentane system as a function of $1/T^*$ for the different loading conditions examined in this work. ● $N_A = 34$, □ $N_A = 90$ and △ $N_A = 159$. (a) Tracer diffusion coefficients and (b) Overall diffusion coefficient.

Table VI Parameters for the Arrhenius equation for the diffusion coefficient as a function of inverse temperature.

	$N_A = 34$	$N_A = 90$	$N_A = 159$
[a] $E_t(neo)$	12.8(6)	13(2)	11.9(8)
[a] $D_0(neo)$	11(2)	15(2)	11(1)
[a] $E_t(n)$	11(2)	11(3)	11(1)
[a] $D_0(n)$	3(3)	7(3)	8(2)

[a] E_t and D_0 were computed from a straight line fit of $\ln(D^*_{1\cdot 1})$ versus $1/T^*$ (see Equation (20)). The activation energy is units of kJ/mol while D_0 is in the same reduced units as the diffusion coefficients in Table V.

purposes. The results obtained are reported in Table VI. The non-Arrhenius behavior observed in Figures 13 and 14 is primarily due to the distinctly different environments in which the more rapidly diffusing molecules find themselves as the temperature is varied. It is clear from the density profiles discussed in section 3.1 that at low T the particles are primarily influenced by the local atomic structure of the silica surface whereas at the highest temperature considered a significant proportion of the molecules are diffusing over comparatively large distances within the void space of the medium. The estimated activation energies are, nonetheless, in fair agreement with the trends expected for alkane/silica systems at low coverages [51]. The close agreement between the activation energies for both neopentane and n-pentane also suggests that the activated state for diffusion of both species may involve the simultaneous passage of three sites over an energy barrier on the silica surface. This was suggested earlier as an explanation for the very slow relaxation of the function P_1 for n-pentane as shown in Figure 12 and is further supported by the results illustrated in Figure 8 for the orientational correlation functions P_1 and P_2 for neopentane. This implies a quasi-sliding motion for the neopentane particles over the solid surface.

In comparing the diffusivities $D^*_{1\cdot 1}$ for the neopentane and n-pentane systems it is observed that at high temperature and low coverage the n-pentane tracer diffusivities are much smaller. At low temperature and high coverage, however, a near-equality exists and the results for D_0 provided in Table VI suggest that these trends are due to the greater influence of the surface screening by preadsorbed material in the case of n-pentane as the surface coverage increases. The results for the overall diffusion coefficient D^*_{AA} on the other hand display a significantly different behavior with higher values for n-pentane at high temperatures and loadings. This transition in the kinetic selectivity of n-pentane relative to neopentane with increasing temperature and coverage is primarily due to the increased admolecule/admolecule interactions involved in the case on n-pentane at high temperatures. At low surface coverages and temperatures the neopentane diffuses more rapidly within the microporous medium due to its weaker interaction with the solid.

Finally, the rotational diffusion coefficients for the neopentane and n-pentane systems are examined for the range of temperatures and loadings considered in this work. For the purposes of brevity, we will refer to both D^*_r and D^*_J as rotational diffusion coefficients and denote them both simply by D^*_r. The values for D^*_r for

neopentane and n-pentane are reported in Table V and it is seen that in both systems there is a dramatic increase in D_r^* with temperature. It is also clear that neopentane is not as rotationally hindered as n-pentane under most temperature and loading conditions although at high temperatures and loadings the values for D_r^* are comparable in magnitude. The reasons for the difference in these results is again due to the weaker interaction involved between the neopentane particles and the silica surface arising from the weak central carbon potential interaction as well as the fact that one of the four methyl sites on the neopentane particles is, on average, located at a greater distance from the solid surface than any of the sites on the n-pentane particles. These observations also complement the results for P_1 and P_2 shown in Figure 8 for neopentane and Figure 12 for n-pentane which demonstrate the much higher degree of rotational hindrance involved in the n-pentane system.

4 CONCLUSIONS

In the present study the effects of molecular structure and flexibility on the transport behavior of alkane vapors adsorbing on microporous silica have been examined. The influence of molecular structure was demonstrated by a comparison of the structureless SF_6 system reported in Ref. [11] with the current investigation of a rigid tetrahedrally structured neopentane system. The major difference lies in the surface backscattering mechanism which appears to be much more significant in the case of structureless particles in contrast to the neopentane molecules. This is in turn reflected in the higher permeation rates observed in the neopentane system under similar conditions. Furthermore, the microporous medium was also examined for its shape selectivity by comparing the spherically symmetric neopentane system with the linear, flexible n-pentane system over a range of pore loading and temperature conditions. At high temperatures, there is a transition in the diffusivities of the overall fluid arising from enhanced diffusion rates in the n-pentane system.

The n-pentane simulations also provide important information with regard to their conformational equilibrium states in an inhomogeneous environment. In all of the simulations conducted the trans/gauche ratio was found to be significantly larger than in the ideal-gas state. Moreover, the bond angle distribution was also found to be much broader, and these results may have an important bearing on heterogeneous catalytic cracking processes.

References

[1] V. Ya. Antonchenko, V. V. Ilyin, N. N. Makoovsky, A. N. Pavlov and V. P. Sokhan, "On the nature of disjoining pressure oscillations in fluid films", *Mol. Phys.*, **52**, 345 (1984).

[2] J. J. Magda, M. Tirrell and H. T. Davis, "Molecular dynamics of narrow, liquid filled pores", *J. Chem. Phys.*, **83**, 1888 (1985).

[3] S. -H. Suh and J. M. D. MacElroy, "Molecular dynamics simulation of hindered diffusion in microcapillaries", *Mol. Phys.*, **58**, 445 (1986).

[4] J. M. D. MacElroy and S. -H. Suh, "Computer simulation of moderately dense hard-sphere fluids and mixtures in microcapillaries", *Mol. Phys.*, **60**, 475 (1987).

[5] U. Heinbuch and J. Fischer, "On the application of Widom's test particle method for homogeneous and inhomogeneous fluids", *Mol. Sim.*, **1**, 109 (1987).

[6] B. K. Peterson, K. E. Gubbins, G. S. Heffelfinger, U. Marini Bettolo Marconi and F. van Swol, "Lennard Jones fluids in cylindrical pores: Nonlocal theory and computer simulations", *J. Chem. Phys.*, **88**, 6487 (1988).
[7] M. Schoen, J. H. Cushman, D. J. Diestler and C. L. Rhykerd, Jr., "Fluid in micropores II. Self diffusion in a simple classical fluid in a slit pore", *J. Chem. Phys.*, **88**, 1394 (1988).
[8] I-A. Park and J. M. D. MacElroy, "Simulation of a hard-sphere fluid in bicontinuous random media", *Mol. Sim.*, **2**, 105 (1989).
[9] J. M. D. MacElroy and S. -H. Suh, "Simulation studies of a Lennard Jones liquid in micropores", *Mol. Sim.*, **2**, 313 (1989).
[10] J. M. D. MacElroy and K. Raghavan, "Adsorption and diffusion of Lennard-Jones vapor in microporous silica", *J. Chem. Phys.*, **93**, 2068 (1990).
[11] J. M. D. MacElroy and K. Raghavan, "Transport of an adsorbing vapour in a model silica system", *J. Chem. Soc., Fara. Trans.*, **13**, 1971 (1991).
[12] J. J. Magda, M. Tirrell and H. T. Davis, "The transport properties of rod-like particles: II narrow slit pore", *J. Chem. Phys.*, **88**, 1207 (1988).
[13] I. Bitsanis and G. Hadziioannou, "Molecular dynamics simulation of the structure and dynamics of confined polymer melts", *J. Chem. Phys.*, **92**, 3827 (1990).
[14] K. Raghavan and J. M. D. MacElroy, "Dynamical studies of translational and rotational hindrance of a needle fluid in random porous media", *Mol. Sim.*, **8**, 93 (1991).
[15] A. Brodka and T. W. Zerda, "Molecular dynamics simulation of reorientational motion of SF_6 in porous sol-gel glass", *J. Non Cryst. Solids*, **139**, 215 (1992).
[16] I. Teraoka, K. H. Langely and F. E. Karasz, "Reptation dynamics of semirigid polymers in porous media", *Macromolecules*, **25**, 6106 (1992).
[17] K. H. Langely, I. Teraoka and F. E. Karasz, "Diffusion of flexible and semirigid polymers confined to the pores spaces in porous glass", *Prog. Colloid Polym. Sci.*, **91**, 153 (1993).
[18] A. G. Bezus, A. V. Kiselev, A. A. Lopatkin and P. Q. Du, "Molecular statistical calculation of the Thermodynamic Adsorption Characteristics of Zeolites using Atom-Atom Approximation" *J. Chem. Soc., Faraday Trans. II*, **74**, 367 (1978).
[19] A. V. Kiselev, A. A. Lopatkin and A. A. Shulga, "Molecular statistical calculation of gas adsorption by silicalite", *Zeolites*, **5**, 261 (1985).
[20] J. P. Ryckaert, G. Cicotti and H. J. C. Berendsen, "Numerical integration of the Cartesian Equations of Motion of a System with Constrains: Molecular dynamics of n-alkanes", *J. Compt. Phys.*, **23**, 327 (1977).
[21] J. P. Ryckaert and A. Bellemans, "Molecular Dynamics of Liquid Alkanes", *Fara. Disc. of Chem. Soc.*, **66**, 95 (1978).
[22] R. Edberg, D. J. Evans and G. P. Morris, "Constrained Molecular Dynamics-Simulation of Liquid Alkanes with a New Algorithm", *J. Chem. Phys.*, **84**, 6933 (1986).
[23] W. L. Jorgensen, J. D. Madura and C. J. Swenson, "Optimized Intermolecular Potential Functions for Liquid Hydrocarbons", *J. Am. Chem. Soc.*, **106**, 6638 (1984).
[24] M. P. Allen and D. J. Tildesley, "Computer Simulations of Liquids", Clarendon Press, Oxford (1987).
[25] M. Karplus, "Molecular dynamics simulations of proteins", *Phys. Today*, **40**, 68 (Oct., 1987).
[26] T. Ichiye, B. D. Olafson, S. Swaminathan and M. Karplus, "Structure and Internal Mobility of Proteins: Molecular Dynamics Study of Hen-egg White Lysozyme", *Biopolymers*, **25**, 1909 (1986).
[27] M. Karplus and J. A. McCammon, "Dynamics of Proteins-Elements and Functions", *Ann. Rev. Biochem.*, **53**, 263 (1983).
[28] T. Ichiye and M. Karplus, "Fluorescence Depolarization of Tryptophan residues in Proteins-Molecular dynamics study", *Biochemistry*, **22**, 2884 (1983).
[29] W. F. van Gunsteren and M. Karplus, "Protein Dynamics in Solution and in a Crystalline Environment: Molecular Dynamics Study", *Biochemistry*, **21**, 2259 (1982).
[30] L. A. McCammon and M. Karplus, "Dynamics of Tyrosine ring rotations in a globular protein", *Biopolymers*, **19**, 1375 (1980).
[31] M. Karplus, "Molecular dynamics of biomolecules overview and applications", *Isr. J. Chem.*, **27**, 121 (1986).
[32] M. Karplus and J. A. McCammon, "Internal dynamics of globular proteins", *CRC Critical Reviews in Biochemistry*, **9**(4), 293 (1981).
[33] W. F. van Gunsteren and M. Karplus, "Effect of Constraints on the Dynamics of Macromolecules", *Macromol.*, **15**, 1528 (1982); *Ibid., Nature*, **293**(5834), 677 (1981).
[34] W. F. van Gunsteren and H. J. C. Berendsen, "Molecular dynamics: perspective for complex systems", *Biochem. Soc. Trans.*, **10**, 301 (1982).
[35] R. G. Gordon, "Molecular Motion in Infrared and Raman Spectra", *J. Chem. Phys.*, **43**, 1307 (1965).

[36] R. G. Gordon, "Relations between Raman Spectroscopy and Nuclear Spin Relaxation", *J. Chem. Phys.*, **42**, 3658 (1965).
[37] B. J. Berne, P. Pechukas and G. D. Harp, "Molecular reorientation in liquids and gases", *J. Chem. Phys.*, **49**, 3125 (1968).
[38] B. J. Berne, "Time-Dependent Properties of Condensed Media", Ch. 9 in *Physical Chemistry-Advanced Treatise*, **8B**, D. Henderson (Ed.), Academic Press, N.Y (1971).
[39] S. Toxvaerd, "Molecular Dynamics of Liquid Butane", *J. Chem. Phys.*, **89**, 3808 (1988).
[40] S. Toxvaerd, "Comment on Constrained Molecular Dynamics of Macromolecules", *J. Chem. Phys.*, **87**, 6140 (1987).
[41] A. Warshel and S. Lifson, "Consistent Force Field Calculation. II Crystal Structures, Sublimation Energies, Molecular and Lattice Vibrations, Molecular Conformations and Enthalpies of Alkanes", *J. Chem. Phys.*, **53**, 582 (1970).
[42] R. L. June, A. T. Bell and D. N. Theodorou, "Molecular Dynamics Study of Methane and Xenon in Silicalite", *J. Phys. Chem.*, **94**, 8232 (1990); *Ibid.*, "Prediction of Low Occupancy Sorption of Alkanes in Silicalite", *J. Phys. Chem.*, **94**, 1508 (1990).
[43] L. J. Lowden and D. Chandler, *J. Chem. Phys.*, **59**, 6587 (1973); *Ibid.*, "Theory of Intermolecular Pair Correlations for Molecular Liquids. Applications to Liquids Carbon Tetrachloride, Carbon Disulphide, Carbon Diselenide, and Benzene" *J. Chem. Phys.*, **61**, 5228 (1974).
[44] D. G. Montague, M. R. Chowdhury, J. C. Dore and J. Reed, "A RISM study of Structural Data for Tetrahedral Molecules", *Mol. Phys.*, **50**, 1 (1983).
[45] T. Keyes and J. Mercer, Physica, "Some Considerations on the Calculation of the Velocity Correlation Function in the Ring Approximation, with Application to the Lorentz Gas", **95A**, 473 (1979).
[46] W. Gotze, E. Leutheusser and S. Yip, "Dynamical Theory of Diffusion and Localization in Random, Static Field", *Phys. Rev. A*, **23**, 2634 (1981).
[47] W. Gotze, E. Leutheusser and S. Yip, "Correlation Functions of the Hard-Sphere Lorentz Model", *Phys. Rev. A*, **24**, 1008 (1981).
[48] A. Masters and T. Keyes, "Diffusion, Percolation, and Trapping in the Lorentz Gas via Variational Kinetic Theory", *Phy. Rev. A*, **26**, 2129 (1982).
[49] M. H. Ernst, J. Machta, J. R. Dorfman and H. van Beijeren, "Long Time Tails in Stationary Random Media. I. Theory", *J. Stat. Phys.*, **34**, 477 (1984).
[50] J. Machta, M. H. Ernst, H. van Beijeren and J. R. Dorman, "Long Time Tails in Stationary Random Media. II Applications", *J. Stat. Phys.*, **35**, 413 (1984).
[51] P. Schneider and J. M. Smith, "Chromatographic Study of Surface Diffusion", *AIChE J.*, 886 (1968).